Biogeosciences Discuss., 9, 10961–11012, 2012
www.biogeosciences-discuss.net/9/10961/2012/
doi:10.5194/bgd-9-10961-2012

Biogeosciences Discussions

Global ocean carbon uptake: magnitude, variability and trends

R. Wanninkhof[1], G.-H. Park[1,2,*], T. Takahashi[3], C. Sweeney[4,16], R. Feely[5], Y. Nojiri[6], N. Gruber[7], S. C. Doney[8], G. A. McKinley[9], A. Lenton[10], C. Le Quéré[11], C. Heinze[12,13,14], J. Schwinger[12,13], H. Graven[7,15], and S. Khatiwala[3]

[1]Ocean Chemistry Division, NOAA/AOML, 4301 Rickenbacker Causeway, Miami FL 33149, USA
[2]Cooperative Institute for Marine and Atmospheric Studies, University of Miami, Miami, FL, USA
[3]Lamont-Doherty Earth Observatory of Columbia University, Route 9W, Palisades NY 10964, USA
[4]NOAA/ESRL Carbon Cycle Group Aircraft Project Lead, 325 Broadway GMD/1 Boulder, CO, USA
[5]Ocean Climate Research Division, NOAA/PMEL, 7600 Sand Point Way NE, Seattle WA 98115, USA
[6]Center for Global Environmental Research National Institute for Environmental Studies Onogawa 16-2, Tsukuba, Ibaraki 305-8506, Japan
[7]Environmental Physics Group, Institute of Biogeochemistry and Pollutant Dynamics, ETH Zurich, 8092 Zurich, Switzerland
[8]Woods Hole Oceanographic Institution, Woods Hole MA, 02543, USA

[9]Atmospheric and Oceanic Sciences and Center for Climatic Research, University of Wisconsin – Madison, WI, USA
[10]CSIRO Marine and Atmospheric Research, P.O. Box 1538 Hobart Tasmania, Australia
[11]Tyndall Centre for Climate Change Research, University of East Anglia, Norwich Research Park, Norwich NR4 7TJ, UK
[12]Geophysical Institute, University of Bergen, Allegaten 70, 5007 Bergen, Norway
[13]Bjerknes Centre for Climate Research, Bergen, Norway
[14]Uni Bjerknes Centre, Uni Research, Bergen, Norway
[15]Scripps Institution of Oceanography, University of California, San Diego, 9500 Gilman Dr., La Jolla, CA, 92093–0244, USA
[16]CIRES, University of Colorado, Boulder, CO 80304, USA
[*]now at: East Sea Research Institute, Korea Institute of Ocean Science & Technology, Uljin, 767-813, Korea

Received: 30 June 2012 – Accepted: 3 July 2012 – Published: 15 August 2012

Correspondence to: R. Wanninkhof (rik.wanninkhof@noaa.gov)

Published by Copernicus Publications on behalf of the European Geosciences Union.

BGD
9, 10961–11012, 2012

Abstract

Estimates of the anthropogenic global-integrated sea-air carbon dioxide (CO_2) flux from 1990 to 2009, based on different models and measurements, range from −1.4 to −2.6 Pg C yr^{-1}. The median values of anthropogenic CO_2 for each method show better agreement and are: −1.9 for Pg C yr^{-1} for numerical ocean general circulation hind cast models (OGCMs) with parameterized biogeochemistry; −2.1 Pg C yr^{-1} for atmospheric inverse models; −1.9 Pg C yr^{-1} for global atmospheric constraints based on O_2/N_2 ratios for 1990–2000; and −2.4 Pg C yr^{-1} for oceanic inverse models. An updated estimate of this anthropogenic CO_2 flux based on a climatology of sea-air partial pressure of CO_2 differences (ΔpCO_2) (Takahashi et al., 2009) and a bulk formulation of gas transfer with wind speed for year 2000 is −2.0 Pg C yr^{-1}. Using this ΔpCO_2 climatology and empirical relationships of pCO_2 with sea-surface temperature (SST) anomalies (Park et al., 2010a), the interannual variability of the contemporary CO_2 flux is estimated to be 0.20 Pg C yr^{-1} (1σ) from 1990 through 2009. This is similar to the variability estimated by the OGCMs of 0.16 Pg C yr^{-1} but smaller than the interannual variability from atmospheric inverse estimates of 0.40 Pg C yr^{-1}. The variability is largely driven by large-scale climate re-organizations. The decadal trends for different methods range from −0.13 (Pg C yr^{-1}) decade^{-1} to −0.50 (Pg C yr^{-1}) decade^{-1}. The OGCMs and the data based sea-air CO_2 flux estimates show smaller uptakes and appreciably smaller decadal trends than estimates based on changes in carbon inventory suggesting that methods capable of resolving shorter timescales are showing a slowing of the rate of ocean CO_2 uptake. It is not clear if this large difference in trend is a methodological issue or a real natural feedback.

1 Introduction

This global analysis of sea-air carbon dioxide (CO_2) fluxes is part of the Regional Carbon Cycle Assessment and Processes (RECCAP) that assesses the input of

BGD
9, 10961–11012, 2012

anthropogenic CO_2 into the atmosphere (Andres et al., 2012) and the fluxes of carbon between the ocean, atmosphere and terrestrial biosphere from 1990 through 2009. The ocean exchanges CO_2 with the atmosphere at the sea-air interface, a process that is driven by a complex and varying set of physical and biogeochemical processes that make accurate assessment of the sea-air CO_2 flux challenging. Improved estimates of the global-integrated net sea-air fluxes are particularly relevant for quantifying the ocean uptake of anthropogenic CO_2 (Sabine and Tanhua, 2010).

The anthropogenic CO_2 perturbation, caused by increasing atmospheric CO_2 levels due to fossil fuel burning and land use changes, is superimposed on the natural CO_2 cycle. While these can be separated in models, measurements provide the combined natural and anthropogenic component, sometimes referred to as the contemporary flux. Exchange of natural CO_2 across the sea-air interface tends to dominate on regional scales (Gruber et al., 2009) but largely cancels at the global scale, with the exception of an outgassing flux of CO_2 that is driven by the input of carbon by rivers (Sarmiento and Sundquist, 1992). The total contemporary flux of CO_2 is the sum of a natural CO_2 flux (including the river-induced outgassing flux) and the anthropogenic CO_2 uptake flux, which is that part of the exchange that is driven by the anthropogenic increase in atmospheric CO_2. Both fluxes vary with time, but for different reasons. The anthropogenic CO_2 flux primarily responds to the increase in atmospheric CO_2, with climate variability having a minor impact (e.g., Lovenduski et al., 2008). In contrast, the natural carbon flux is not impacted by the rise in atmospheric CO_2, but can change substantially in response to climate (Le Quéré et al., 2010).

Different approaches are used to estimate the ocean carbon sink. The net sea-air CO_2 flux across the sea-air interface provides a direct estimate. Micro-meteorological techniques such as the eddy-covariance method of CO_2 (Fairall et al., 2000) can determine sea-air CO_2 fluxes directly at local scale but with significant uncertainty, preventing a meaningful extrapolation to larger scales. At regional to global scale a bulk flux expression is used that has a kinetic term and thermodynamic term according to:

$$F = k \times (C_w - C_a) \quad (1)$$

BGD
9, 10961–11012, 2012

where the kinetic term, k, is called the gas transfer velocity and incorporates all processes that control the kinetics of the gas transfer across the sea-air interface, while the term ($C_w - C_a$) is the concentration gradient of the gas in the liquid boundary layer that is on the order of 100 micron thick. For sea-air CO_2 fluxes the equation is commonly written in terms of the partial pressure (or fugacity) difference across the interface according to:

$$F = k \times K_0 \times (pCO_{2w} - pCO_{2a}) = k \times K_0 \times \Delta pCO_2 \quad (2)$$

where the convention is that a net flux into the ocean is expressed as negative value. pCO_{2w} is the partial pressure of CO_2 of surface water, pCO_{2a} is the partial pressure of CO_2 in air, K_0 is the solubility of CO_2, and ΔpCO_2 is the partial pressure gradient ($\Delta pCO_2 = pCO_{2w} - pCO_{2a}$). The CO_2 levels in air are reported as a mixing ratio or mole fraction, XCO_{2a} which must be converted to a partial pressure through $pCO_{2a} = XCO_{2a}\,(P - p_{H_2O})$, where P is the ambient pressure and p_{H_2O} is the saturation pressure of water vapor.

An observational approach to estimating the sea-air flux of CO_2 is to make measurements of ΔpCO_2 from ships and moorings. Other approaches used to infer global sea-air CO_2 fluxes rely on models, total inorganic carbon measurements in the ocean interior and/or atmospheric data. Of these methods, those relying on simulations with Ocean General Circulation Models (OGCMs) with parameterization of biogeochemical processes calculate the CO_2 flux using Eq. (2). In this case, pCO_{2w} is computed from the modeled state variables of the carbonate system; total alkalinity (TAlk) and total dissolved inorganic carbon (DIC). The resolution of global biogeochemical models used in RECCAP is on the order 2 by 2 degree with output provided at monthly scales (e.g., Canadell et al., 2012). Oceanic inverse models constrain the regional and global fluxes from interior ocean circulation and ocean interior data based on measurements of DIC and other tracers (Mikaloff Fletcher et al., 2006, 2007; Gruber et al., 2009), with the advantage of estimating both the natural and anthropogenic CO_2 flux components on decadal scales. The inverse estimates are independent of the estimates

BGD
9, 10961–11012, 2012

based on ΔpCO_2 (Eq. 2). Khatiwala et al. (2009, 2012) provide estimates of changes in anthropogenic CO_2 in the ocean interior using a Green function with transient tracers that yields the anthropogenic CO_2 uptake estimates at regional scales. Atmospheric inversions use atmospheric transport models and measured atmospheric CO_2 levels to assess sources and sinks of contemporary CO_2, i.e., the sum of natural and anthropogenic CO_2. Faster atmospheric transport and mixing leads to coarser spatial resolution but higher temporal resolution compared to ocean inversions with about a dozen ocean regions (Jacobson et al., 2007). Trends in the atmospheric ratio of O_2 / N_2 along with atmospheric CO_2 levels can be used to separate terrestrial CO_2 uptake from that of oceanic uptake due to reservoir specific fractionation (Manning and Keeling, 2006). Scales of ocean uptake estimates are hemispheric and monthly depending on the level of sophistication of interpretation.

Data based estimates of variability and trends in ocean CO_2 uptake are limited by the short record of observations. High quality measurements in the surface water and air commenced in the early 1960's but at limited scope (Fig. 1). Global physical forcing fields such as wind speeds are available for the last 5 decades, but the older estimates are inconsistent with current measurements due to large changes in observing and interpolation methods.

In this overview the focus is on the last 20 yr (1990–2009) with the recognition that the first decade has data limitations. The emphasis is on the ΔpCO_2 observations and empirical approaches that are based heavily on observations of surface ocean temperature. These are compared with models and observations of anthropogenic CO_2 and other tracers in the ocean interior. The background section is a summary of measured variability and trends as well as current global-integrated carbon cycle inventories and fluxes. The methodology describes an empirical approach to estimate a 20-yr time series of global-integrated sea-air fluxes from the global pCO_2 climatology, sea surface temperature (SST) and wind anomalies over the past two decades, and a procedure to incorporate the effect of increasing atmospheric CO_2 levels. It discusses the different models and other approaches used in the analysis. In the discussion we will focus

BGD
9, 10961–11012, 2012

on the anthropogenic flux and detail adjustments between the different modeling and observational approaches to get consistent estimates. In the last section the estimates are reconciled for a consistent global anthropogenic CO_2 uptake. It concludes with a summary of the median anthropogenic CO_2 uptake, and the sub-annual and interannual variability of the net sea-air CO_2 fluxes.

2 Background

2.1 Atmospheric CO_2 variability and trends

The pCO_2 of air (pCO_{2a}) is well constrained from measurement of the mole fraction of CO_2, XCO_2, in air at about 80 global flask sampling stations worldwide (Conway et al., 1994). Seasonal changes of approximately 10 ppm over the Northern hemisphere ocean are driven by the photosynthesis and respiration cycle of the terrestrial biosphere. Much smaller seasonal changes are observed in the Southern Hemisphere due to the lack of land cover. The atmospheric CO_2 measurements point towards rapid zonal atmospheric mixing (weeks to month) and impedance in the tropics causing slower north-south inter-hemispheric exchanges on the order of a year (Denning et al., 2002). Superimposed on the natural cycle is the increase in CO_2 concentration from burning of fossil fuel and land-use changes, the anthropogenic perturbation. These changes are largely driven from the Northern Hemisphere with bleed-over in the atmospheric CO_2 signal to the Southern Hemisphere on annual timescales, leading to a substantial north-to-south gradient in the annual mean XCO_2. Roughly half of the anthropogenic CO_2 emissions accumulate in the atmosphere, causing an average increase in CO_2 concentration of 1.8 ppm yr^{-1} from 1990 through 2009.

BGD
9, 10961–11012, 2012

2.2 Oceanic pCO_{2w} variability and trends

In contrast to the atmospheric pCO_2, the pCO_2 in the surface ocean (pCO_{2w}) is spatially and temporally more variable, and therefore requires several orders of magnitude more data to map variation (Figs. 1 and 2). Seasonal and interannual changes can be 100 µatm or more. The spatial decorrelation length scales are on the order of 100's of km (Li et al., 2005) compared to 1000's of km in the marine atmosphere. The greater variability and challenges in making measurements of pCO_{2w} means that for large parts of the ocean there are insufficient observations to obtain direct estimates of ΔpCO_2 everywhere (Fig. 2). Only select regions such as the equatorial Pacific, and time-series stations in the sub-tropical North Atlantic (ESTOC and BATS) and sub-tropical North Pacific (HOT) have sufficient measurements and robust interpolation schemes to discern decadal variability and trends based on observations alone.

Two approaches have been pursued to overcome this limitation. The most commonly used approach is to collate the data to form a monthly global climatology of ΔpCO_2 (Takahashi et al., 2009), henceforth referred to as T-09. The T-09 climatology is constructed from approximately 3 million data points obtained over the last 40 yr, assuming that the ΔpCO_2 does not vary on multi-year timescales. The climatology is on coarse (4° latitude × 5° longitude) resolution, and data have been interpolated over the annual cycle and in space using the mean surface flow fields from an OGCM. The second approach is to interpolate the data in time and space using ancillary observations, such as SST, mixed layer depth and other (remotely sensed) surface parameters. No global estimate is yet available based on this approach, but self-organizing maps (Telszewski et al., 2009) and multi-parameter regressions (Schuster, McKinley et al., 2012) have been used to determine regional ΔpCO_2 fields and fluxes.

For variability and trends over the past two decades for the global ocean we are limited to numerical models and a scheme that utilizes the monthly pCO_2 climatology of T-09 and local-scale empirical relationships of pCO_{2w} against SST. These empirical

BGD
9, 10961–11012, 2012

relationships are then applied to the more comprehensive, time-varying SST record to arrive at monthly estimates (Park et al., 2010a) as detailed below.

2.3 Global ocean CO_2 uptake estimates

Various "best estimates" of ocean anthropogenic CO_2 uptake have been reported based on a variety of data and methods. The 4th IPCC Assessment (Table 1; Denman et al., 2007) provide estimates for the 1980s and 1990s on the basis of measurements of ΔpCO_2 (Takahashi et al., 2009), ocean inversions of oceanic data (Mikaloff Fletcher et al., 2006), atmospheric inversions, carbon isotopic mass balances (Gruber and Keeling, 2001; Quay et al., 2003) and atmospheric O_2/N_2 measurements (Bender et al., 2005; Manning and Keeling, 2006), while that for the 2000–2005 period is based on model results.

More recently, long-term trends of ocean uptake of CO_2 determined by models have been reported in the literature (e.g., Le Quéré et al., 2007; Sarmiento et al., 2010) and regularly updated as part of the Global Carbon Project (GCP) (Le Quéré et al., 2009; www.globalcarbonproject.org/). The estimates consider mass balances and fluxes among all major labile reservoirs (ocean, atmosphere, and terrestrial biosphere). The annual model-based estimate for the net air-sea CO_2 flux since 1960 is provided in Fig. 3. These results suggest that despite the fact that the ocean sink has increased significantly over the past 50 yr, the increase is slower than the increase in fossil fuel emissions. Thus the percent of fossil fuel emissions absorbed by the oceans had steadily declined.

The treatment of the different air-sea CO_2 flux components in modeling approaches represent a substantial challenge when comparing different flux estimates. Our aim here is to focus on the anthropogenic component of the CO_2 flux, which we compute from estimates of the contemporary CO_2 flux by subtracting the natural CO_2 flux component. The latter can be estimated if we assume that ocean circulation and biological activity has remained roughly constant over the last 250 yr. In this case, this flux, when integrated over the globe, cancels to zero except for the river-carbon induced

BGD
9, 10961–11012, 2012

outgassing flux of CO_2. Although this assumption provides a good first estimate, we need to recognize that interannual variability and trends in circulation and biogeochemistry cause temporal fluctuations in the natural CO_2 flux components. Most of these deviations are believed to occur on interannual time-scales, such that decadal averages of the natural CO_2 flux component are less than $\pm 0.3\,\mathrm{Pg\,C\,yr^{-1}}$ (Lovenduski et al., 2008). The decadal trends in circulation and biogeochemistry are less well known and could cause changes in the decadal trends of sea-air CO_2 fluxes.

The contribution of the river-carbon induced outgassing flux of CO_2 amounts to about $+0.45\,\mathrm{Pg\,C\,yr^{-1}}$ (Jacobson et al., 2007) and needs to be accounted for when comparing model simulation results with estimates based on ΔpCO_2 measurements and Eq. 2. The river efflux is believed to be relatively constant through time, so that a constant offset of $0.5\,\mathrm{Pg\,C\,yr^{-1}}$ is applied to the net sea-air CO_2 fluxes based on ΔpCO_2 to obtain the anthropogenic CO_2 flux. Additional adjustments are to compare different estimates and include surface area of the ocean used, sea-ice, and coastal carbon input.

The Takahashi et al. (2009) (T-09) ΔpCO_2 climatology is used as an observational benchmark for the net contemporary or net sea-air CO_2 fluxes, and it is the basis for our empirical approach to estimate interannual variability. However, even with over 3 million data points and its coarse resolution, the T-09 pCO_{2w} climatology is data limited. For much of the ocean, particularly the Southern Hemisphere, the seasonal cycle cannot be fully resolved from measurements alone. As shown in Fig. 2, only in the Northern Hemisphere are there sufficient monthly observations to create a full climatological year. A propagation of errors suggests an uncertainty in the global fluxes from the climatology of 50 %. However, the estimated fluxes are in better than 50 % agreement with independent mass balance and model estimates (e.g., Gruber et al., 2009). The adjustments and breakdown of errors are listed in Table 2 along with an updated estimate.

The uncertainty estimates in Table 2 are described in Sect. 6.4 of Takahashi et al. (2009). The breakdown of the uncertainty estimate shows that the smallest

BGD
9, 10961–11012, 2012

uncertainty in global sea-air CO_2 fluxes is associated with the ΔpCO_2 estimate. This mirrors the conclusion for a regional estimate by Watson et al. (2009) that the large de-correlation length scales of hundreds of kilometers and the large number of measurements in each grid cell increase the certainty in ΔpCO_2 appreciably. However, the uncertainty estimate in ΔpCO_2 does not fully account for the dearth of measurements in many parts of the ocean. The uncertainty in the gas transfer velocity, k, is based on the range of common parameterizations presented in the literature. Recent syntheses suggest that globally the uncertainty in gas transfer is in the range of 10 to 20 % (Ho et al., 2011). Differences in global wind products are substantial, but this is partially compensated for by normalizing gas transfer-wind speed relationships to match global ocean bomb-^{14}C inventories (Sweeney et al., 2007; Naegler, 2009). As described above, the uncertainty estimates are not rigorous but rather based on best knowledge. Moreover, some of uncertainties are likely to be systematic and cannot be propagated in the simple fashion shown in Table 2.

The largest uncertainty in the global CO_2 flux climatology of T-09 is attributed to the assumption that the surface seawater pCO_2 increases at the same rate as the atmospheric CO_2 levels of $\approx 1.5\,\mathrm{ppm\,yr^{-1}}$ for the past four decades. The uncertainty estimate of $\pm 0.5\,\mathrm{Pg\,C\,yr^{-1}}$ is derived from assuming an uncertainty of $\pm 0.5\,\mu\mathrm{atm\,yr^{-1}}$ in the oceanic CO_2 increase accounting for the data distribution in time. Therefore, the assumption that the ΔpCO_2 remains invariant is critical for the climatology. For regional shorter term assessments, where data are not normalized to a common time reference, this uncertainty does not come into play.

The rate of CO_2 gas exchange is much faster than exchange of CO_2 between the mixed layer and the waters below (Broecker and Peng, 1982). On a global scale the surface ocean CO_2 levels should keep up with the atmosphere albeit with a lag of about $-0.1\,\mu\mathrm{atm\,yr^{-1}}$, assuming an average gas transfer velocity of $16\,\mathrm{cm\,h^{-1}}$, a Revelle factor of 10, an average mixed layer of 50 m and an atmospheric increase of $1.5\,\mathrm{ppm\,yr^{-1}}$ (Broecker and Peng, 1982). This estimate is similar to a more comprehensive representation in OGCMs when the atmospheric CO_2 is increasing at a rate as observed

BGD
9, 10961–11012, 2012

but other surface forcing and circulation remains constant, a so-called CO_2-only run (Le Quéré et al., 2010).

Using the dataset assembled for T-09, McKinley et al. (2011) and Le Quéré et al. (2010) show that for several regions of the ocean the ΔpCO_2 does not remain constant over periods of up to three decades. This is attributed to circulation changes, and possibly changes in the biological cycle. The Southern Ocean (Le Quéré et al., 2007; Lovenduski et al., 2008; Lenton and Matear, 2007; Lenton et al., 2012) and Eastern North Atlantic (Schuster et al., 2007; Omar and Olsen, 2006; Metzl et al., 2010) show that surface water pCO_{2w} has increased faster than atmospheric CO_2, thereby decreasing the CO_2 sink. In the Southern Ocean where the changes are attributed to more upwelling of deep-water the changes are believed to be sustained. Increased upwelling is attributed to increases in zonal wind stress caused by large-scale reorganizations of the southern hemisphere climate system in response to global warming and stratospheric ozone loss (Thompson and Solomon, 2002). In other parts of the ocean, where the changes are attributed to more ephemeral causes, no systematic long-term changes in uptake are anticipated, as of yet, other than those caused by increasing atmospheric CO_2 levels.

Winds have a major impact on sea-air CO_2 fluxes through their influence on k (Eq. 2). Long-term global wind records suggest an increase with time (Young et al., 2011) The global wind speed records are either based on atmospheric assimilations commonly used in weather forecasts, ship and buoy based observations, remotely sensed winds, or a combination thereof. Determining accurate trends is challenging because of changes in procedures and inputs. Assimilation model outputs (e.g., NCEP, ECMWF) are re-analyzed, often with a major objective to eliminate procedural biases. The reanalysis products show appreciable global and regional differences in magnitude and variability (Wallcraft et al., 2009). For the RECCAP analysis the cross-calibrated multiplatform (CCMP) winds are used as they address many of the shortcomings of other products for the determination of sea-air CO_2 fluxes. The product is well documented and consistent for the entire time record (Atlas et al., 2011). The CCMP product, which

BGD
9, 10961–11012, 2012

covers the time period from 1 January 1990 through 31 December 2009, shows appreciable trends in wind speed over time both regionally and globally. Figure 4 shows the trends of the second moment of the winds, $\langle U^2 \rangle$, used in the analyses (see Eq. 3). At 90 % significance level the trends show decreases in $\langle U^2 \rangle$ in the Subtropical North Pacific and increases in the Southern Ocean and Equatorial Pacific. The increasing winds have a direct effect on the sea-air CO_2 flux through an impact on the gas transfer velocity but also an indirect effect on ΔpCO_2 from changes in ocean circulation and mixed layer dynamics.

3 Methods

Here we provide details on the bulk flux equation (Eq. 2) input parameters, which are key for surface ocean data-based methods and OGCMs that provide fluxes based on ΔpCO_2. The procedure to determine a 20-yr time record of fluxes from SST anomalies is provided. The OGCMs, atmospheric and ocean inverse models, and estimates based on atmosphere O_2 / N_2 are described briefly.

3.1 Gas transfer velocities and wind speeds

The global CO_2 flux estimate reported in T-09 used the NCEP-II assimilated wind speed product. The NCEP-II product is inconsistent in magnitude and wind speed pattern over the ocean compared to other products (Fig. 5) (Wallcraft et al., 2009). For the observation-based estimate in RECCAP, the cross-calibrated multiplatform (CCMP) winds (Atlas et al., 2011) were chosen instead as the default product. The second moments of the winds were determined from the 6-hourly observations at the spatial resolution of 0.25° from the data at available at http://podaac.jpl.nasa.gov/DATA_CATALOG/ccmpinfo.html.

Using these second moments and an inverse procedure to optimize the inventory of bomb-^{14}C in the ocean (Sweeney et al., 2007), the coefficient for the gas transfer

BGD
9, 10961–11012, 2012

velocity, a, is determined:

$$k = a\langle U^2 \rangle \quad (3)$$

where k is the gas transfer velocity (cm h^{-1}), "$\langle\ \rangle$" denote temporal averages, and $\langle U^2 \rangle$ in (m s^{-1})^2 is the time-mean of the second moment of the wind speed at 10-m height. The coefficient a was adjusted such that the bomb-^{14}C inventory increase in the ocean corresponded with the atmospheric ^{14}C history. The optimal coefficient for the gas transfer velocity parameterization is:

$$k = 0.251(\mathrm{Sc}/660)^{-0.5}\langle U^2 \rangle \quad (4)$$

where Sc is the Schmidt number of CO_2 in seawater at a given SST. The relationship of Sc for CO_2 with SST in seawater is: $\mathrm{Sc} = 2073.1 - 125.62 \times \mathrm{SST} + 3.6276 \times \mathrm{SST}^2 - 0.043219 \times \mathrm{SST}^3$ (Wanninkhof, 1992). Other relationships between k and wind speed have been proposed but for the prevailing wind speed range from 4–12 m s^{-1} a quadratic appears appropriate for global scale analyses (Wanninkhof et al., 2009).

3.2 Updated gas transfer velocity parameterization and impact on global fluxes

The CCMP wind product averaged over the 4° × 5° grid used by T-09 yields a global average, 20-yr mean, wind speed $\langle U \rangle$ of 7.6 m s^{-1} and a second moment, $\langle U^2 \rangle$ of 69.1 (m s^{-1})^2. Using Eq. (4) this yields a global average gas transfer velocity $\langle k \rangle$ of 15.95 cm h^{-1}, and a global sea-air CO_2 flux of −1.18 Pg C yr^{-1} when applied to the Takahashi ΔpCO_2 climatology (downloaded October 2010 from: http://www.ldeo.columbia.edu/res/pi/CO2/carbondioxide/pages/air_sea_flux_2010.html). For comparison the net sea-air flux, without the under sampling correction, determined by T-09 using NCEP-II winds is −1.38 Pg C yr^{-1} (Table 2).

BGD
9, 10961–11012, 2012

3.3 Method for estimating decadal variability and trends in ΔpCO_2 using a data based approach

There are limited observational data on global trends and variability in ocean sea-air CO_2 fluxes. An empirical approach first presented in Lee et al. (1998) and improved in Park et al. (2010a), henceforth referred to as P-10, provides an assessment of interannual variability from seasonal correlations of pCO_{2w} and SST that are used with the measured interannual SST variability. This approach is applied to the T-09 climatology as follows: The monthly mean sea-air CO_2 flux for each $4^\circ \times 5^\circ$ grid cell for an individual year other than the climatological year 2000 is estimated from the global pCO_{2w} climatology, and pCO_{2w} anomalies determined from sub-annual pCO_{2w}-SST relationships. The sub-annual pCO_{2w}-SST relationships are derived from one to four linear fits of pCO_{2w} and SST for each of the 1759 $4^\circ \times 5^\circ$ grid cells in the T-09 climatology. The number of sub-annual segments chosen to delineate the sub-annual trends is kept to the minimum sufficient to characterize the relationship between pCO_{2w} and SST for each location. The monthly $\langle U^2 \rangle$ is from CCMP, and the monthly mean SST is from the NOAA Optimum Interpolation (OI) SST product (Reynolds et al., 2007; http://www.cdc.noaa.gov/data/gridded/data.noaa.oisst.v2.html). Sea level pressures from NCEP-II for each grid cell are used to determine the pCO_{2a} from the measured XCO_{2a}. Details are provided in Park et al. (2010b).

For the central and eastern Equatorial Pacific (6° N–10° S and 80° W–165° E) empirical pCO_{2w}-SST equations are derived from a large quantity of multi-year observations that were collected from 1979 through 2008 (updated from Feely et al., 2006). Based on the observations over the last several decades it is clear that the drivers of interannual variability in this region are different from those of seasonal variability. For the period of investigation, covering seven El Niño and five La Nina periods, unique pCO_{2w}-SST equations for three different time periods (1979–1989, 1990–mid-1998, and mid-1998–2008) are used that reflect the modulation of ENSO by the Pacific Decadal Oscillation

BGD
9, 10961–11012, 2012

(PDO). Using these relationships the interannual variability based on the annual values for this region is 0.07 Pg C yr^{-1} (1σ) for the 1990–2009 time period.

The empirical method of P-10 to assess interannual variability is implicitly tied to the ΔpCO_2 climatology referenced to year 2000 such that is cannot reproduce trends tied to increasing atmospheric CO_2 levels. Changes in biogeochemistry of surface seawater associated with SST changes will be reflected as long as the same mechanisms that relate sub-annual pCO_{2w} change to SST control the interannual pCO_{2w}-SST relationships. A weak increasing trend in pCO_{2w}, associated with surface ocean warming is estimated by the P-10 method over the 20-yr period. This leads to a reduction in net global ocean CO_2 uptake (see below).

The P-10 method implicitly assumes that pCO_{2w} increases at the same rate as atmospheric CO_2 levels, that is the ΔpCO_2 remains constant over time. The "CO_2-only" run of NCAR CCSM-3 model (Doney et al., 2009a, b) for the period of 1987–2006 is used to determine local deviations in this trend. This model output is produced using a repeat annual cycle of physical forcing and rising atmospheric CO_2. In each $4^\circ \times 5^\circ$ grid cell, the trend in pCO_{2w} is computed by a linear regression with de-seasonalized monthly values using a harmonic function. Approximately 75 % of the grid cells have statistically significant positive or negative trends in ΔpCO_2 ($p < 0.05$) over the past two decades. For the remaining 25 % of the grid cells with no significant trends, we assume that pCO_{2w} increases at the same rate as atmospheric CO_2. From these trends the "CO_2-only" fluxes are determined for each grid cell and are added to CO_2 fluxes from the empirical model to estimate the total flux over 1990–2009. Global maps of the trends of the CO_2-only output, using a different model but with similar results, can be found in Fig. 4b of Le Quéré et al. (2010).

3.4 Ocean global circulation models (OGCMs)

The trends and variability observed in the models result are caused by changing physical forcing and the resulting changes in circulation and biogeochemistry. A list of the OGCMs used in RECCAP is shown in Table 3. The model output and metadata used

BGD
9, 10961–11012, 2012

in the discussion are provided at the RECCAP website, with model details given in Canadell et al. (2012). Of the 9 model runs provided in RECCAP, several are from the same model but with different gas exchange or wind forcing. Only the LSC and UEA models include the input of riverine carbon but the input does not appear to contribute to subsequent outgassing. Therefore, the flux estimates from all models used here are the anthropogenic CO_2 component and the natural CO_2 flux component, which without riverine carbon outgassing is globally nearly balanced (≈ 0).

3.5 Other estimates of global sea-air CO_2 fluxes

Several other global estimates are compared that rely on changes in atmospheric or oceanic anthropogenic CO_2 inventories. These include results from eleven atmospheric inverse models provided by RECCAP, atmospheric O_2/N_2, and ocean inventory changes using transient tracers and a Green function analysis. Atmospheric inversions are based on the interpretation of atmospheric CO_2 gradients, but given the under constrained nature of this inversion, they need prior information for the sea-air CO_2 fluxes, for which CO_2 flux climatologies such as that of T-09 are used as priors. As a result, these estimates are net fluxes and include all flux components, i.e., natural (with river outgassing) and anthropogenic. As they use the observed sea-air flux as a prior they are not a truly independent estimate. In contrast, the O_2/N_2 approach provides a strong independent constraint for the anthropogenic CO_2 flux component only. Estimates from 1989–2003 can be found in Manning and Keeling (2006); while results from 2000–2010 are presented in Ishidoya et al. (2012). The anthropogenic CO_2 fluxes inferred from changing oceanic inventories are further detailed in Khatiwala et al. (2012). Briefly, they include an empirical Green function approach (Khatiwala et al., 2009, 2012) and a model-based approach, commonly referred to as the ocean inversion project (OIP) (Mikaloff Fletcher et al., 2006; Gruber et al., 2009). These approaches are based on the assumption of a steady-state ocean circulation and therefore only resolve the smoothly evolving changes in the oceanic uptake of anthropogenic

BGD
9, 10961–11012, 2012

CO_2 driven by the increase in atmospheric CO_2, i.e., they do not resolve interannual and sub-annual variability.

4 Discussion

4.1 Global sea-air CO_2 fluxes

A tabular summary of the decadal mean anthropogenic CO_2 uptake centered on the year 2000 and based on several observation based techniques and models is provided in Table 4 with further detail below. Also shown are the interannual variability (IAV), sub-annual variability (SAV), and trends of the net sea-air CO_2 flux. The interannual and subannual variability is dominated by the natural CO_2 flux, and the trend is primarily caused by the anthropogenic component with modulation by the natural cycle.

4.1.1 Anthropogenic sea-air CO_2 flux estimate based on surface water measurements

The empirical estimates in Table 4 follow the procedures and assumptions of T-09 and P-10. The main differences are the wind speed product used, the use of the second moment of the wind speed, and the coefficient in the gas transfer parameterization. The fluxes are extrapolated to include the coastal regions.

Despite using the same constraints and consistent assumptions as T-09, the difference of 0.19 Pg C yr^{-1} (Table 2) arises because of spatial differences in wind speed products and cross-correlations between direction of flux and wind (Wanninkhof et al., 2009). The T-09 global anthropogenic CO_2 flux estimate does not include coastal regions. Fluxes in coastal area are highly variable but net fluxes on the whole appear similar to that of adjacent ocean areas, with some regional exceptions, particularly along Eastern upwelling zones that show large effluxes near the coast, and riverine dominated shelves that show influxes (Chavez et al., 2007; Liu et al., 2010; Cai, 2011). For the global analysis we scaled-up fluxes from each of the 23 ocean regions by the

BGD
9, 10961–11012, 2012

difference in areas as provided in T-09 and the total area as used in the OIP (Supplement A), These corrections yield an anthropogenic CO_2 flux of $-2.0\,Pg\,C\,yr^{-1}$ that is the same as the $-2.0\,Pg\,C\,yr^{-1}$ presented in T-09. However, as outlined in Table 2 the lower uptake in the open ocean is compensated for by incorporating the coastal areas. The reduced uncertainty of $0.6\,Pg\,C\,yr^{-1}$ compared to $0.8\,Pg\,C\,yr^{-1}$ in T-09 is due to improvements in the estimate of gas transfer velocities and winds.

4.1.2 Anthropogenic CO_2 uptake estimates based on models and atmospheric observations

Several modeling and atmospheric observing approaches report smaller uncertainties than those relying on measured surface CO_2 levels and bulk flux approaches. An important consideration when determining uncertainties based on multi-model comparisons is that models are often similar, which can lead to an unrealistic good correspondence between them. Graphical summaries of the annual anthropogenic sea-air CO_2 fluxes for the OGCMs and ocean inverse estimates, and the atmospheric inversions are presented in Figs. 6 and 7, respectively. A summary of the medians of different methods is shown in Fig. 8.

4.1.3 Ocean inversion estimates

Ocean inversions rely on inorganic carbon measurements in the ocean interior and can only provide an average anthropogenic sea-air CO_2 flux, interpolated to present day, based on cumulative anthropogenic CO_2 uptake since the preindustrial era. A comprehensive ocean inversion estimate of CO_2 uptake based on a suite of ten general ocean circulation models is presented in Gruber et al. (2009). This inversion value is independent from the bulk sea-air CO_2 flux estimate but contains other potential sources of error associated with the partitioning of anthropogenic from natural dissolved inorganic carbon as well as the potential for biases due to inaccurate estimates of ocean circulation. The inversion-based estimate has a reported uncertainty of $\pm 0.3\,Pg\,C\,yr^{-1}$,

BGD
9, 10961–11012, 2012

determined from the spread of model results. The uncertainty in ocean transport and mixing is the largest source of uncertainty for the ocean inversion. The average anthropogenic CO_2 uptake by the inversions provided in RECCAP is an update of Mikaloff Fletcher et al. (2006) and Gruber et al. (2009) with results shown in Fig. 6. Specifically, the reported values for 1994 were scaled by a factor of 1.109 and 1.23 for the years 2000 and 2005, respectively, based on the scaling used in the inversion procedure itself (Mikaloff Fletcher et al., 2006). The globally integrated anthropogenic sea-air fluxes for nominally for 1995, 2000 and 2005 are -2.18 ± 0.25 and -2.42 ± 0.28 and -2.68 ± 0.31 (1σ) Pg C yr^{-1}, respectively.

Jacobson et al. (2007) present a comprehensive joint inversion scheme applying both atmospheric inverse and oceanic inverse constraints that include an observation based bulk sea-air CO_2 flux estimates modified from Takahashi et al. (2002). The resulting contemporary sea-air fluxes are heavily weighted towards the (interior) oceanic inverse due to the large number of data points and sluggish circulation/transport compared to the atmosphere. As a result, it yields results similar to Gruber et al. (2009) for the contemporary fluxes, implying an anthropogenic flux of -2.1 Pg C yr^{-1} for the time period from 1992–1996 with an uncertainty of ± 0.2 Pg C yr^{-1}. This uncertainty is lower than that of Gruber et al. (2009) primarily because of the use of a smaller set of general circulation models.

4.1.4 Ocean General Circulation Models with biogeochemistry (OGCMs)

A comprehensive synthesis of model performance on a previous generation of carbon cycle OGCMs was provided as part of the OCMIP (Ocean Carbon-Cycle Model Intercomparison Project) in the early 2000s (see e.g., Doney et al., 2004). A more recent subset of models was used to determine the ocean sink for 1959–2008 (Le Quéré et al., 2009; Sarmiento et al., 2010). Initialization, forcing and biological representation differs for the models (Canadell et al., 2012). The models were run in hindcast mode, i.e., they were driven by atmospheric forcing assimilation products such as NCEP or

BGD
9, 10961–11012, 2012

ECWMF, and prescribed atmospheric CO_2 concentration using an observation based product such as GLOBALVIEW-CO2 (2011).

Two things stand out in the time series of annual CO_2 fluxes from OGCMs (Fig. 6). The models with a heritage traceable to the NCAR community ocean circulation model with biogeochemistry (BEC, ETH_{k15}, and ETH_{k19}) show about 0.5 Pg C yr^{-1} less uptake than the others. The UEA models are adjusted to the best observationally-based estimate of ocean uptake in the 1990s and therefore show a mean of anthropogenic CO_2 uptake about −2.2 Pg C yr^{-1}. The second significant difference is the response of the models to major climate reorganizations. The 1997/1998 El Niño was one of the largest on record (see e.g., http://www.esrl.noaa.gov/psd/enso/mei/) with an expected net increase in ocean uptake due to reduced outgassing of CO_2 in the equatorial Pacific (Feely et al., 2006). The models show greatly varying responses in CO_2 fluxes in phasing, magnitude and duration. The NCAR models show a peak-to-peak change of 0.2 Pg C yr^{-1} while the UEA models show peak-to-peak changes of up to 1.0 Pg C yr^{-1}. The Bergen model shows no global response to the El Niño while the CSI shows an increase over several years. Park et al. (2010a) (P-10) estimate an anomaly of about 0.3 Pg C yr^{-1} with a recovery in less than 2 yr (Figs. 8 and 10).

For the estimate of the median anthropogenic CO_2 uptake of the OGCMs, we excluded model outputs that were largely similar and only differed in their forcing. That is, only one of the three UEA model outputs (UEA_{NCEP}) and one of the two ETH (ETH_{k15}) model outputs were used. The solid red line in Fig. 6 is the annual median of LSC, UEA_{NCEP}, CSI, BER, BEC and ETH_{k15} runs. The interannual variability of the median estimate of 0.16 (1σ) Pg C yr^{-1} is damped compared the mean interannual variability of the individual models of 0.25 (1σ) Pg C yr^{-1} indicating that the variability in the individual models is not coherent. The median estimates of the 6 models shows significant trend of -0.14 ± 0.02 Pg C yr^{-1} $decade^{-1}$ ($p < 0.01$) in anthropogenic CO_2 uptake. This trend agrees with the trends of the individual models.

BGD
9, 10961–11012, 2012

4.1.5 Atmospheric inverse models

Ocean anthropogenic uptake determined from atmospheric inverse models shows a similar range as the uptake in the OGCMs with a median value of $-2.1\,\mathrm{Pg\,C\,yr^{-1}}$ (Table 4; Fig. 8). This is similar to the median of the OGCMs and the flux is $0.3\,\mathrm{Pg\,C\,yr^{-1}}$ less than that of the ocean inversion model. The interannual variability is considerably greater ($0.40\,\mathrm{Pg\,C\,yr^{-1}}$, 1σ of detrended median values of de-seasonalized monthly anomalies).

As with the OGCMs, the response of the fluxes from the atmospheric inversions to the 1998 El Niño varies appreciably from no impact to about $1.0\,\mathrm{Pg\,C\,yr^{-1}}$. However, the atmospheric inversions that give a response show the maximum uptake a year earlier (1997). The atmospheric inversions separate the seasonal and interannual CO_2 flux of the ocean from that of the terrestrial biosphere which show sub-annual variability in CO_2 uptake and release that is up to orders of magnitude greater. Therefore the uncertainty of the separation between ocean and terrestrial carbon fluxes dictates the variability in the ocean. The time-averaged global-integrated anthropogenic CO_2 flux from the atmospheric inversions is not independent since the ΔpCO_2 fields used in the CO_2 flux climatology are used as a prior within the inversion. No estimate of the decadal trend is provided as the model runs from which the median estimate is determined differ in time span and time period.

4.2 Trends and variability in wind, ΔpCO_2 and fluxes

The trends and variability in fluxes as determined from the bulk flux equation (Eq. 2) are driven by changes in wind and ΔpCO_2. The trends and variability are discussed in the context of the empirical approach in Park et al. (2010a). The impact of changing winds is different for OGCMs as they are dynamic in nature and higher winds will not only change the rate of gas exchange, but also the ΔpCO_2 field. This can result in decreased net flux through enhanced upwelling of remineralized CO_2 (Le Quéré et al.,

BGD
9, 10961–11012, 2012

2007; Lovenduski et al., 2008). In contrast, applying higher winds to a static ΔpCO_2 field such as the T-09 climatology will result in increased uptake.

4.2.1 Sub-annual (seasonal) variability: seasonal and regional patterns

Interannual variability and trends in CO_2 fluxes are masked by large sub-annual (seasonal) changes on regional scales in ΔpCO_2 and in wind. Thus, the detection of interannual and decadal changes requires a long time-series of measurements. Moreover, variability will differ for different ocean regions as detailed in the chapters of individual basins. Here we provide a zonal analysis of mean and spatial-temporal variability for the global ocean of wind, ΔpCO_2, and the sea-air CO_2 flux density, i.e., the flux per unit area. Figure 9 shows the 20-yr zonal mean and standard deviation of zonal mean for $\langle U^2 \rangle^{0.5}$ and flux density (in mol m^{-2} mo^{-1}), along with the climatological annual zonal mean and standard deviation of the monthly ΔpCO_2 climatology. The second moment of the winds show low winds in the tropics and steady increases towards higher southern and northern latitudes with relatively constant values in the subtropical high pressure regions around 30° N and 30° S. The Southern Ocean experiences higher $\langle U^2 \rangle^{0.5}$ than the northern oceans (11 m s^{-1} vs. 10 m s^{-1}). At latitudes greater than 60° wind speeds decrease slightly. The variance pattern of winds, expressed as the standard deviation in the 20-yr mean in Fig. 9a, differs appreciably between the northern and southern hemisphere. There is appreciably more variability in winds in the mid- to high-latitudes (> 30°) in the Northern Hemisphere than in the Southern Hemisphere. Variability is at a minimum in the high-pressure regimes in the sub-tropics, and at the equator.

The annual mean ΔpCO_2 from the T-09 climatology (Fig. 9b) shows maximum values just south of the equator and a decline to the north and south. The ΔpCO_2 equals approximately 0 near 18–20° and reaches a minimum of −20 to −25 µatm at 40° for both hemispheres. At high northern latitudes the average ΔpCO_2 continues to drop precipitously while in the Southern Hemisphere it increases and, on climatological annual average, becomes slightly positive near the Antarctic ice edge. The variance in ΔpCO_2

BGD
9, 10961–11012, 2012

in the Northern Hemisphere is appreciably greater than in the Southern Hemisphere, as is the case with the wind speeds as well.

The flux density, computed from 20-yr wind speed record and the climatological pCO_2, mirrors the trends in ΔpCO_2 but with amplification at mid-latitudes due to higher winds. The largest sink per unit area is in the Northern Hemisphere, but the substantially larger surface area in the Southern Hemisphere causes a much greater spatially integrated mass exchange (see, Table 6 in T-09). Because the variance in wind speed and ΔpCO_2 have the same pattern, the flux density at mid- to high- latitudes in the Northern Hemisphere show twice the variance in their sub-annual patterns compared to the Southern Hemisphere.

The greater sub-annual CO_2 flux variability in the Northern Hemisphere compared to the Southern Hemisphere is likely because of the significantly greater landmasses in the north. The land-ocean contrast, along with continental input and bathymetry causes greater variability in weather systems, (micro) nutrient input and seasonal temperature variations in the North, all which contribute to higher variability in sea-air CO_2 flux density.

The T-09 climatology excludes the coastal ocean (approximately < 200 km from land) such that much of the area with particularly high variability in ΔpCO_2 and fluxes are excluded (e.g., Borges et al., 2005; Chavez et al., 2007; Liu et al., 2010; Cai, 2011). Several open ocean regions are anomalous compared to the zonal view as described in the ocean basin chapters. These include high sub-annual variability in the seasonal upwelling region in the Arabian Sea caused by the monsoonal winds. High standard deviations from the annual mean of the sea-air CO_2 fluxes are also found in the eastern tropical South Pacific, again attributed to variations in upwelling along the western boundary, and in the southwest Atlantic near the Malvinas confluence area that is impacted by variation in currents, shallow bathymetry and associated plankton blooms. Low sub-annual variability is seen in the subtropical and sub-polar region of the South-East Pacific and Eastern tropical and subtropical South Pacific.

BGD
9, 10961–11012, 2012

4.2.2 Interannual variability

The patterns of sub-annual variability differ from the interannual variability for parts of the oceans as shown in Supplement B. There is high sub-annual and interannual variability in the North Atlantic; in contrast, the Equatorial Pacific shows relatively small sub-annual variability but large interannual variability caused by the ENSO that operates on inter-annual time scales. For large parts of the subtropical gyres the ratio of interannual to sub-annual variability is small ($\approx < 0.2$) indicating that variability on seasonal timescales dominates. In the equatorial and high latitude areas the ratio is greater than 0.4 and in places reaches over 1.0 indicating that interannual variability exceeds sub-annual changes. The regions with high interannual variability correspond with those strongly affected by climate reorganizations; the North Atlantic Oscillation (NAO) in the North Atlantic; the El Niño/Southern Oscillation (ENSO) in the Equatorial Pacific and Equatorial Indian Ocean; and the Southern Annual Mode (SAM) in the Southern Ocean.

4.2.3 Temporal trends in pCO_2

The pCO_{2w} tracks atmospheric pCO_{2a} increases on longer timescales because the surface ocean is closely coupled with the lower atmosphere through rapid sea-air gas exchange and relatively slower exchange between the surface mixed layer and waters below. Longer-term, secular trends in ΔpCO_2 can arise from changes in circulation and upwelling patterns, and associated changes in biological productivity. The longer-term trends are impacted by the rapid rise in atmospheric CO_2, finite uptake capacity of the surface mixed layer, and decreasing buffer capacity. In a fractional sense, these factors lead to a diminished uptake of anthropogenic CO_2 by the ocean while in absolute sense the amount of fossil fuel derived CO_2 taken up by the ocean increases (Fig. 3). This robust result is apparent in most models.

The trend in the global annual flux for the empirical approach, not accounting for atmospheric CO_2 increase, is 0.07 ± 0.06 (Pg C yr^{-1}) decade^{-1} (Figs. 10a and 11d).

BGD
9, 10961–11012, 2012

This decreasing uptake, in the absence of an atmospheric CO_2 increase, suggests that a strengthening of ocean CO_2 sources or weakening of CO_2 sinks, due to changes of ΔpCO_2 or wind speed. The second moment of the wind speed increases by 0.32 ± 0.04 $(m\,s^{-1})^2$ per year, which translates into about a $0.2\,m\,s^{-1}$ increase per decade (Fig. 11a). Global SST as determined from the NOAA OI SST product (Reynolds et al., 2007) shows an increasing trend of 0.08 ± 0.03 $(°C\,yr^{-1})$ $decade^{-1}$ (Fig. 11b). The trends in SST impact the ΔpCO_2 and wind will impact gas transfer in the P-10 approach. An analyses holding the SST or wind constant in the P-10 approach indicate that the changes in the wind and SST can act synergistically or antagonistically on the trend in fluxes depending on region. For example, at high Northern latitudes the trends in winds and SST cause a larger CO_2 sink over the past two decades; in the Equatorial Pacific the impact of winds and SST cause a larger CO_2 source; while in the Southern Ocean the change in ΔpCO_2 due to changing SST will decrease the sink while the winds work in an opposing fashion.

The global trends in sea-air CO_2 flux are strongly influenced by significant interannual variability in ΔpCO_2 (Fig. 11c). In particular, the large El Niños in 1992/1993 and 1998 decreased the equatorial ΔpCO_2 and thus has the net effect of increasing the global-integrated net CO_2 flux into the ocean. This suggests that climate reorganizations on multi-annual timescales have an appreciable impact on the trends over the 2-decade time period.

4.3 Summary of global anthropogenic sea-air CO_2 fluxes and trends in models

Most models show trends of increasing anthropogenic CO_2 uptake from 1990 through 2009 (or 2007). The median for the empirical approach, OGCMs, and atmospheric inversions all show a consistent change in the anthropogenic CO_2 uptake of -0.13 to -0.15 $(Pg\,C\,yr^{-1})$ $decade^{-1}$ over the time period, that is the same as that inferred from the approach in P-10 when including the atmospheric CO_2 increases. Khatiwala et al. (2009, 2012) estimate an increase of inventory change of

BGD
9, 10961–11012, 2012

−0.35 (Pg C yr^{-1}) decade^{-1} based on inventory changes in anthropogenic CO_2 using a Green function formulated from transient tracers. By construction, the Green function approach uptake is smooth, monotonic over time, and proportional to the atmospheric CO_2 increase (Fig. 8).

The median anthropogenic sea-air CO_2 fluxes for the different models for 1990–2009 provided in Table 4 show a good agreement despite different approaches and constraints. The median values are centered on, or determined for, 2000, and they are within their estimated uncertainties. The approaches differ appreciably in their interannual variability (IAV), sub-annual variability (SAV) and trend. The decadal trends differ by a factor of four. Approaches that implicitly or explicitly incorporate contemporary changes in physics and biogeochemistry show much smaller trends than those that use ocean interior data under assumptions of a linear response of the ocean uptake to the atmospheric perturbation, and assumed constant ocean circulation. It is not possible to conclusively determine the best trend estimate given the methodological imperfections of each approach.

The relatively short time scale to determine the trends and large, and variable interannual and sub-annual variability can appreciably bias the decadal trends determined. The IAV, SAV are appreciable compared to the trends and therefore the method of inferring the trends from the OGCMs, and atmospheric and ocean inverse medians can also impact the results. Here, IAV values are calculated as a standard deviation of the 12 monthly median values from de-seasonalized monthly anomalies. SAV values are estimated as a standard deviation of 12 monthly mean values.

While median uptakes for different methods agree, there are appreciable differences within different types of models. Here we compare the OGCMs. Some the model differences are due to different forcing, transport or representation of the ocean carbon cycle, others are caused by more mundane issues such as estimates of global ocean surface area and conversion of areal representations or different representation of sea ice. This is shown in Supplement A where the outputs of the OGCMs are normalized for area by determining the average flux in each the 23 surface regions of the ocean

BGD
9, 10961–11012, 2012

inversion and then integrating over the area of each of the regions as provided in RECCAP. It leads to adjustments up to 0.4 Pg C and better agreement between model runs.

There are also appreciable differences in the interannual and sub-annual variability for the OGCM outputs (Table 5). Sub-annual variability is a standard deviation of 20-yr mean monthly values. Interannual variability is a standard deviation of the detrended values of de-seasonalized monthly anomalies.

5 Conclusions

A re-assessment of the sea-air CO_2 flux based on the ΔpCO_2 climatology of Takahashi et al. (2009) (T-09), and the average 20-yr CCMP wind product, including adjustments for undersampling, coastal areas, riverine inputs and El Niño impacts, yields an anthropogenic flux of $-2.0\,\mathrm{Pg\,C\,yr^{-1}}$ with an uncertainty of $0.6\,\mathrm{Pg\,C\,yr^{-1}}$. Using an empirical approach relating ΔpCO_2 to SST changes according to Park et al. (2010a) (P-10) together with model output including the effect of increasing atmospheric CO_2 levels, leads to a small decadal trend of -0.15 ($\mathrm{Pg\,C\,yr^{-1}}$) $\mathrm{decade^{-1}}$, indicating an increasing sink over the past two decades. These results are in good agreement with median anthropogenic CO_2 uptake for 2000 and decadal trends for 6 OGCMs of $-1.9\,\mathrm{Pg\,C\,yr^{-1}}$ and -0.14 ($\mathrm{Pg\,C\,yr^{-1}}$) $\mathrm{decade^{-1}}$, and the median 12 Atmospheric Inversions of $-2.1\,\mathrm{Pg\,C\,yr^{-1}}$ and -0.13 ($\mathrm{Pg\,C\,yr^{-1}}$) $\mathrm{decade^{-1}}$. The anthropogenic CO_2 uptake primarily based on interior measurements shows slightly greater anthropogenic CO_2 uptake, but within the uncertainty of other measurements. However it shows significantly greater trends. Khatiwala et al. (2009, 2012) provide an anthropogenic CO_2 uptake of $-2.2\,\mathrm{Pg\,C\,yr^{-1}}$ and a decadal trend of -0.35 ($\mathrm{Pg\,C\,yr^{-1}}$) $\mathrm{decade^{-1}}$. Ocean inversions show an uptake for 2000 of $-2.4\,\mathrm{Pg\,C\,yr^{-1}}$ and a prescribed trend -0.5 ($\mathrm{Pg\,C\,yr^{-1}}$) $\mathrm{decade^{-1}}$. As the ocean interior estimates reflect changes over longer timescales, the difference in trends for the different methods could be caused by the decreasing efficiency in ocean uptake with time. However, the trends over the two decades are influenced by variability which is dominated by large-scale interannual

BGD
9, 10961–11012, 2012

variability IAV in sources and sinks which do not show up in the ocean interior estimates.

Supplementary material related to this article is available online at: http://www.biogeosciences-discuss.net/9/10961/2012/bgd-9-10961-2012-supplement.pdf.

Acknowledgements. We wish to thank Joaquin Triñanes for processing the CCMP wind data. RW, G-H. P., RAF were supported in part through the Global Carbon Data Management and Synthesis Project of the NOAA Climate Program Office. NG and HG were supported by funds from ETH Zurich and through the FP7 projects CarboChange (Project reference 264879) and GeoCarbon. CS was supported by NSF/OPP 0944761. SCD acknowledges support through the NOAA Climate Process Team activity, NOAA grant NA07OAR4310098. CH and J S were supported through EU FP7 project COMBINE (grant agreement no. 226520), the Research Council of Norway funded project CarboSeason (185105/S30), and the Norwegian Metacenter for Computational Science and Storage Infrastructure (NOTUR and Norstore, "Biogeochemical Earth system modeling" projects nn2980k and ns2980k).

References

Andres, R. J., Boden, T. A., Bréon, F.-M., Ciais, P., Davis, S., Erickson, D., Gregg, J. S., Jacobson, A., Marland, G., Miller, J., Oda, T., Olivier, J. G. J., Raupach, M. R., Rayner, P., and Treanton, K.: A synthesis of carbon dioxide emissions from fossil-fuel combustion, Biogeosciences, 9, 1845–1871, doi:10.5194/bg-9-1845-2012, 2012.

Assmann, K. M., Bentsen, M., Segschneider, J., and Heinze, C.: An isopycnic ocean carbon cycle model, Geosci. Model Dev., 3, 143–167, doi:10.5194/gmd-3-143-2010, 2010.

Atlas, R., Hoffman, R. N., Ardizzone, J., Leidner, S. M., Jusem, J. C., Smith, D. K., and Gombos, D.: A cross-calibrated multiplatform ocean surface wind velocity product for meteorological and oceanographic applications, B. Am. Meteorol. Soc., 92, 157–174, doi:10.1175/2010BAMS2946.1, 2011.

BGD
9, 10961–11012, 2012

Aumont, O. and Bopp, L.: Globalizing results from ocean in situ iron fertilization studies, Global Biogeochem. Cy., 20, GB2017, doi:10.1029/2005GB002591, 2006.
Bender, M. L., Ho, D. T., Hendricks, M. B., Mika, R., Battle, M. O., Tans, P. P., Conway, T. J., Sturtevant, B., and Cassar , N.: Atmospheric O_2/N_2 changes, 1993–2002: Implications for the partitioning of fossil fuel CO_2 sequestration, Global Biogeochem. Cy., 19, GB4017, doi:10.1029/2004GB002410, 2005.
Borges, A. V., Delille, B., and Frankignoulle, M.: Budgeting sinks and sources of CO_2 in the coastal ocean: Diversity of ecosystems counts, Geophys. Res. Lett., 32, L14601 doi:10.11029/12005GL023053, 2005.
Broecker, W. S. and Peng, T.-H.: Tracers in the Sea, Eldigio Press, Palisades, 690 pp., 1982.
Buitenhuis, E. T., Rivkin, R. B., Sailley, S., and Quéré, C. L.: Biogeochemical fluxes through microzooplankton, Global Biogeochem. Cy., 24, GB4015, doi:10.1029/2009GB003601, 2010.
Cai, W.-J.: Estuarine and coastal ocean carbon paradox: CO_2 sinks or sites of terrestrial carbon incineration, Annu. Rev. Mar. Sci., 3, 123–145, doi:10.1146/annurev-marine-120709-142723, 2011.
Canadell, J. G., Ciais, P., Le Quere, C., Luyssaert, S., Raupach, R., and Sitch, S.: REgional Carbon Cycle Assessment and Processes (RECCAP): Methods and Data, Biogeosciences, in preparation, 2012.
Chavez, F., Takahashi, T., Cai, W.-J., Friederich, G. E., Hales, B. E., Wanninkhof, R., and Feely, R. A.: The Coastal Ocean, in: The First State of the Carbon Cycle Report (SOCCR): The North American Carbon Budget and Implications for the Global Carbon Cycle, edited by: King, A. W., Dilling, L., Zimmerman, G. P., Fairman, D. M., Houghton, R. A., Marland, G., Rose, A. Z., and Wilbanks, T. J., Chapter 15, Report by the US Climate Change Science Program and the Subcommittee on Global Change Research, National Oceanic and Atmospheric Administration, National Climatic Data Center, Asheville, NC, USA, 157–166, 2007.
Conway, T. J., Tans, P. P., Waterman, L. S., Thoning, K. W., Kitzis, D. R., Masarie, K. A., and Zhang, N.: Evidence for interannual variability of the carbon cycle from the NOAA/CMDL global air sampling network, J. Geophys. Res., 99, 22831–22855, 1994.
Denman, K. L. and Brasseur, G.: Couplings Between Changes in the Climate System and Biogeochemistry, in: IPCC, Climate Change 2007: The Physical Science Basis, Contribution of Working Group I to the Fourth Assessment Report of the Intergovernmental Panel on Climate Change edited by: Solomon, S., Qin, D., Manning, M., Chen, Z., Marquis, M., Averyt,

BGD
9, 10961–11012, 2012

K., Tignor, M., and Miller, H., Cambridge University Press, Cambridge, United Kingdom, 2007.
Denning, A. S. and Fung, I. Y.: Latitudinal gradient of atmospheric CO_2 due to seasonal exchange with land biota, Nature, 376, 240–243, doi:10.1038/376240a0, 2002.
Doney, S., Lindsay, K., Caldeira, K., Campin, J.-M., Drange, H., Dutay, J.-C., Follows, M., Gao, Y., Gnanadesikan, A., Gruber, N., Ishida, A., Joos, F., Madec, G., Maier-Reimer, E., Marshall, J. C., Matear, R. J., Monfray, P., Mouchet, A., Najjar, R., Orr, J. C., Plattner, G.-K., Sarmiento, J., Schlitzer, R., Slater, R., Totterdell, I. J., Weirig, M.-F., Yamanaka, Y., and Yool, A.: Evaluating global ocean carbon models: the importance of realistic physics, Global Biogeochem. Cy., 18, GB3017, doi:10.1029/2003GB002150, 2004.
Doney, S. C., Lima, I., Feely, R. A., Glover, D. M., Lindsay, K., N.Mahowal, Moore, J. K., and Wanninkhof, R.: Mechanisms governing interannual variability in the upper ocean inorganic carbon system and air-sea CO_2 fluxes, Deep-Sea Res. Pt. II, 56, 640–655, 2009a.
Doney, S. C., Lima, I., Moore, J. K., Lindsay, K., Behrenfeld, M. J., T.K. Westberry, Mahowald, N., Glover, D. M., and Takahashi, T.: Skill metrics for confronting global upper ocean ecosystem-biogeochemistry models against field and remote sensing data, J. Mar. Syst., 76, 95–112, doi:10.1016/j.jmarsys.2008.05.015, 2009b.
Fairall, C. W., Hare, J. E., Edson, J. B., and McGillis, W.: Parameterization and micrometeorological measurement of air-sea gas transfer, Bound.-Lay. Meteorol., 96, 63–105, 2000.
Feely, R. A., Takahashi, T., Wanninkhof, R., McPhaden, M. J., Cosca, C. E., and Sutherland, S. C.: Decadal variability of the air-sea CO_2 fluxes in the equatorial pacific ocean, J. Geophys. Res., 111, CO8S90 doi:10.1029/2005JC003129, 2006.
GLOBALVIEW-CO2 2011: Cooperative Atmospheric Data Integration Project – Carbon Dioxide, CD-ROM, NOAA ESRL, Boulder, Colorado online at: ftp.cmdl.noaa.gov, path: ccg/co2/GLOBALVIEW, 2011.
Graven, H. D., Gruber, N., Key, R., Khatiwala, S., and Giraud, X.: Changing controls on oceanic radiocarbon: New insights on shallow-to-deep ocean exchange and anthropogenic CO_2 uptake, J. Geophys. Res., in revision, 2012.
Gruber, N. and Keeling, C. D.: An improved estimate of the isotopic air-sea disequilibrium of CO_2: Implications for the oceanic uptake of anthropogenic CO_2, Geophys. Res. Lett., 28, 555–558, 2001.
Gruber, N., Gloor, M., Fletcher, S. E. M., Doney, S. C., Dutkiewicz, S., Follows, M. J., Gerber, M., Jacobson, A. R., Joos, F., Lindsay, K., Menemenlis, D., Mouchet, A., Muller, S. A., Sarmiento,

BGD
9, 10961–11012, 2012

J. L., and Takahashi, T.: Oceanic sources, sinks, and transport of atmospheric CO_2, Global Biogeochem. Cy., 23, GB1005, doi:10.1029/2008GB003349, 2009.
Ho, D. T., Wanninkhof, R., Schlosser, P., Ullman, D. S., Hebert, D., and Sullivan, K. F.: Towards a universal relationship between wind speed and gas exchange: Gas transfer velocities measured with $^3He/SF_6$ during the Southern Ocean Gas Exchange Experiment, J. Geophys. Res., 116, C00F04, doi:10.1029/2010JC006854, 2011.
Ishidoya, S., Aoki, S., Goto, D., Nakazawa, T., Taguchi, S., and Patra, P. K.: Time and Space variations of O_2/N_2 ratio in the troposphere over Japan and estimation of the global CO_2 budget for the period 2000–2010, Tellus B, 64, 18964, doi:10.3402/tellusb.v64i0.18964, 2012.
Jacobson, A. R., Mikaloff-Fletcher, S. E., Gruber, N., Sarmiento, J. S., and Gloor, M.: A joint atmosphere-ocean inversion for surface fluxes of carbon dioxide: 1. Methods and global-scale fluxes, Global Biogeochem. Cy., 21, GB1019, doi:10.1029/2005GB002556, 2007.
Khatiwala, S., Primeau, F., and Hall, T.: Reconstruction of the history of anthropogenic CO_2 concentrations in the ocean, Nature, 462, 346–349 doi:10.1038/nature08526, 2009.
Khatiwala, S., Tanhua, T., Mikaloff Fletcher, S., Gerber, M., Doney, S. C., Graven, H. D., Gruber, N., McKinley, G. A., Murata, A., Ríos, A. F., Sabine, C. L., and Sarmiento, J. L.: Global ocean storage of anthropogenic carbon, Biogeosciences Discuss., 9, 8931–8988, doi:10.5194/bgd-9-8931-2012, 2012.
Le Quéré, C., Röedenbeck, C., Buitenhuis, E. T., Conway, T. J., Langenfelds, R., Gomez, A., Labuschagne, C., Ramonet, M., Nakazawa, T., Metzl, N., and Gillett, N.: Saturation of the Southern ocean CO_2 sink due to recent climate change, Science, 316, 1735–1738, doi:10.1126/science.1136188, 2007.
Le Quéré, C., Raupach, M. R., Canadell, J. G., Marland, G., Bopp, L., Ciais, P., Conway, T. J., Doney, S. C., Feely, R. A., Foster, P., Friedlingstein, P., Gurney, K., Houghton, R. A., House, J. I., Huntingford, C., Levy, P. E., Lomas, M. R., Majkut, J., Metzl, N., Ometto, J. P., Peters, G. P., Prentice, I. C., Randerson, J. T., Running, S. W., Sarmiento, J. L., Schuster, U., Sitch, S., Takahashi, T., Viovy, N., Werf, G. R. v. d., and Woodward, F. I.: Trends in the sources and sinks carbon dioxide, Nat. Geosci., 2, 831–836, doi:10.1038/ngeo689, 2009.
Le Quéré, C., Takahashi, T., Buitenhuis, E. T., Rödenbeck, C., and Sutherland, S. C.: Impact of climate change and variability on the global oceanic sink of CO_2, Global Biogeochem. Cy., 24, GB4007, doi:10.1029/2009GB003599, 2010.
Lee, K., Wanninkhof, R., Takahashi, T., Doney, S., and Feely, R. A.: Low interannual variability in recent oceanic uptake of atmospheric carbon dioxide, Nature, 396, 155–159, 1998.

BGD
9, 10961–11012, 2012

Lenton, A. and Matear, R. J.: Role of the southern annular mode (SAM) in Southern Ocean CO_2 uptake, Global Biogeochem. Cy., 21, GB2016, doi:10.1029/2006GB002714, 2007.
Lenton, A., Metzl, N., Takahashi, T., Kuchinke, M., Matear, R., Roy, T., Sutherland, S. C., Sweeney, C., and Tilbrook, B.: The observed evolution of oceanic pCO_2 and its drivers over the last two decades, Global Biogeochem. Cy., 26, GB2021, doi:10.1029/2011GB004095, 2012.
Li, Z., Adamec, D., Takahashi, T., and Sutherland, S. C.: Global aurocorrelation scales of the partial pressure of oceanic CO_2, J. Geophys. Res., 110, C08002, doi:10.1029/2004JC002723, 2005.
Liu, K.-K., Atkinson, L., Quinones, R., and Talaue-McManus, L. (Eds.): Carbon and nutrient fluxes in continental margins, Springer, Heidelberg, 741 pp., 2010.
Lovenduski, N. S., Gruber, N., and Doney, S. C.: Toward a mechanistic understanding of the decadal trends in the Southern Ocean carbon sink, Global Biogeochem. Cy., 22, GB3016, doi:10.1029/2007GB003139, 2008.
Manning, A. C. and Keeling, R. F.: Global oceanic and land biota sinks from the Scripps atmospheric oxygen flask sampling network, Tellus B, 58, 95–116, 2006.
Matear, R. J. and Lenton, A.: Impact of historical climate change on the Southern Ocean carbon cycle, J. Climate, 21, 5820–5834, 2008.
McKinley, G. A., Fay, A. R., Takahashi, T., and Metzl, N.: Convergence of atmospheric and North Atlantic carbon dioxide trends on multidecadal timescales, Nat. Geosci., 4, 606–610, doi:10.1038/NGEO1193, 2011.
Metzl, N., Corbiere, A., Reverdin, G., Lenton, A., Takahashi, T., Olsen, A., Johannessen, T., Pierrot, D., Wanninkhof, R., Olafsdottir, S. R., Olafsson, J., and Ramonet, M.: Recent acceleration of the sea surface fCO_2 growth rate in the North Atlantic subpolar gyre (1993–2008) revealed by winter observations, Global Biogeochem. Cy., 24, GB4004, doi:10.1029/2009GB003658, 2010.
Mikaloff Fletcher, S. E., Gruber, N., Jacobson, A. R., Doney, S. C., Dutkiewicz, S., Gerber, M., Follows, M., Joos, F., Lindsay, K., Menemenlis, D., Mouchet, A., Muller, S. A., and Sarmiento, J. L.: Inverse estimates of anthropogenic CO_2 uptake, transport, and storage by the ocean, Global Biogeochem. Cy., 20, GB2002, doi:10.1029/2005GB002530, 2006.
Mikaloff Fletcher, S. E., Gruber, N., Jacobson, A. R., Doney, S. C., Dutkiewicz, S., Gerber, M., Gloor, M., Follows, M., Joos, F., Lindsay, K., Menemenlis, D., Mouchet, A., Müller, S. A., and Sarmiento, J. L.: Inverse estimates of the oceanic sources and sinks

BGD
9, 10961–11012, 2012

of natural CO_2 and the implied oceanic transport, Global Biogeochem. Cy., 21, GB1010, doi:10.1029/2006GB002751, 2007.
Naegler, T.: Reconciliation of excess ^{14}C-constrained global CO_2 piston velocity estimates, Tellus B, 61, 372–384, 2009.
Omar, A. M. and Olsen, A.: Reconstructing the time history of the air-sea CO_2 disequilibrium and its rate of change in the eastern subpolar North Atlantic, 1972–1989, Geophys. Res. Lett., 33, L04602, doi:10.1029/2005GL025425, 2006.
Park, G.-H., Wanninkhof, R., Doney, S. C., Takahashi, T., Lee, K., Feely, R. A., Sabine, C., Triñanes, J., and Lima, I.: Variability of global net sea-air CO_2 fluxes over the last three decades using empirical relationships, Tellus B, 62, 352–368, doi:10.1111/j.1600-0889.2010.00498.x, 2010a.
Park, G.-H., Wanninkhof, R., and Triñanes, J.: Procedures to Create Near Real-Time Seasonal Air-Sea CO_2 Flux Maps Atlantic Oceanographic and Meteorological Laboratory NOAA Technical Memorandum-98, OAR AOML, Miami, 21, 2010b.
Quay, P. D., Sonnerup, R., Westby, T., Stutsman, J., and McNichol, A.: Anthropogenic changes of the $^{13}C/^{12}C$ of dissolved inorganic carbon in the ocean as a tracer of CO_2 uptake, Global Biogeochem. Cy., 17, 1004, doi:10.1029/2001GB001817, 2003.
Reynolds, R. W., Smith, T. M., Liu, C., Chelton, D. B., Casey, K. S., and Schlax, M. G.: Daily high-resolution blended analyses for sea surface temperature, J. Climate, 20, 5473–5496, 2007.
Sabine, C. L. and Tanhua, T.: Estimation of anthropogenic CO_2 inventories in the ocean, Annu. Rev. Mar. Sci., 2, 175–198, doi:10.1146/annurev-marine-120308-080947, 2010..
Sarmiento, J. L. and Sundquist, E. T.: Revised budget for the oceanic uptake of anthropogenic carbon dioxide, Nature, 356, 589–593, 1992.
Sarmiento, J. L., Gloor, M., Gruber, N., Beaulieu, C., Jacobson, A. R., Mikaloff Fletcher, S. E., Pacala, S., and Rodgers, K.: Trends and regional distributions of land and ocean carbon sinks, Biogeosciences, 7, 2351–2367, doi:10.5194/bg-7-2351-2010, 2010.
Schuster, U. and Watson, A. J.: A variable and decreasing sink for atmospheric CO_2 in the North Atlantic, J. Geophys. Res., 112, C11006, doi:10.1029/2006JC003941, 2007.
Schuster, U., McKinley, G. A., Bates, N., Chevallier, F., Doney, S. C., Fay, A. R., González-Dávila, M., Gruber, N., Jones, S., Krijnen, J., Landschützer, P., Lefèvre, N., Manizza, M., Mathis, J., Metzl, N., Olsen, A., Rios, A. F., Rödenbeck, C., Santana-Casiano, J. M., Taka-

BGD
9, 10961–11012, 2012

hashi, T., Wanninkhof, R., and Watson, A. J.: Atlantic and Arctic sea-air CO_2 fluxes, 1990–2009, Biogeosciences Discuss., 9, 10669–10724, doi:10.5194/bgd-9-10669-2012, 2012.

Solomon, S., Qin, D., Manning, M., Alley, R. B., Berntsen, T., Bindoff, N. L., Chen, Z., Chidthaisong, A., Gregory, J. M., Hegerl, G.C., Heimann, M., Hewitson, B., Hoskins, B. J., Joos, F., Jouzel, J., Kattsov, V., Lohmann, U., Matsuno, T., Molina, M., Nicholls, N., Overpeck, J., Raga, G., Ramaswamy, V., Ren, J., Rusticucci, M., Somerville, R., Stocker, T. F., Whetton, P., Wood R. A., and Wratt, D.: Technical Summary, in: Climate Change 2007: The Physical Science Basis, Contribution of Working Group I to the Fourth Assessment Report of the Intergovernmental Panel on Climate Change, edited by: Solomon, S., Qin, D., Manning, M., Chen, Z., Marquis, M.,. Averyt, K. B, Tignor M., and Miller, H. L., Cambridge University Press, Cambridge, United Kingdom and New York, NY, USA, 2007.

Sweeney, C., Gloor, E., Jacobson, A. R., Key, R. M., McKinley, G., Sarmiento, J. L., and Wanninkhof, R.: Constraining global air-sea gas exchange for CO_2 with recent bomb C-14 measurements, Global Biogeochem. Cy., 21, GB2015, doi:10.1029/2006GB002784, 2007.

Takahashi, T., Sutherland, S. G., Sweeney, C., Poisson, A. P., Metzl, N., Tilbrook, B., Bates, N. R., Wanninkhof, R., Feely, R. A., Sabine, C. L., Olafsson, J., and Nojjiri, Y.: Global sea-air CO_2 flux based on climatological surface ocean pCO_2, and seasonal biological and temperature effects, Deep-Sea Res. Pt. II, 49, 1601–1622, 2002.

Takahashi, T., Sutherland, S. C., Wanninkhof, R., Sweeney, C., Feely, R. A., Chipman, D. W., Hales, B., Friederich, G., Chavez, F., Sabine, C., Watson, A., Bakker, D. C. E., Schuster, U., Metzl, N., Inoue, H. Y., Ishii, M., Midorikawa, T., Nojiri, Y., Koertzinger, A., Steinhoff, T., Hoppema, M., Olafsson, J., Arnarson, T. S., Tilbrook, B., Johannessen, T., Olsen, A., Bellerby, R., Wong, C. S., Delille, B., Bates, N. R., and de Baar, H. J. W.: Climatological mean and decadal change in surface ocean pCO_2, and net sea-air CO_2 flux over the global oceans, Deep-Sea Res. Pt. II, 554–577, doi:10.1016/j.dsr2.2008.12.009, 2009.

Telszewski, M., Chazottes, A., Schuster, U., Watson, A. J., Moulin, C., Bakker, D. C. E., González-Dávila, M., Johannessen, T., Körtzinger, A., Lüger, H., Olsen, A., Omar, A., Padin, X. A., Ríos, A. F., Steinhoff, T., Santana-Casiano, M., Wallace, D. W. R., and Wanninkhof, R.: Estimating the monthly pCO_2 distribution in the North Atlantic using a self-organizing neural network, Biogeosciences, 6, 1405–1421, doi:10.5194/bg-6-1405-2009, 2009.

Thompson, D. W. J. and Solomon, S.: Interpretation of recent Southern Hemisphere climate change, Science, 296, 895–899, doi:10.1126/science.1069270, 2002.

BGD
9, 10961–11012, 2012

Wallcraft, A. J., Kara, A. B., Barron, C. N., Metzger, E. J., Pauley, R. L., and Bourassa, M. A.: Comparisons of monthly mean 10-m wind speeds from satellites and NWP products over the global ocean, J. Geophys. Res., 114, D16109, doi:10.1029/2008JD011696, 2009.

Wanninkhof, R.: Relationship between gas exchange and wind speed over the ocean, J. Geophys. Res., 97, 7373–7381, 1992.

Wanninkhof, R., Asher, W. E., Ho, D. T., Sweeney, C. S., and McGillis, W. R.: Advances in quantifying air-sea gas exchange and environmental forcing, Annu. Rev. Mar. Sci., 1, 213–244, doi:10.1146/annurev.marine.010908.163742, 2009.

Watson, A. J., Schuster, U., Bakker, D. C. E., Bates, N. R., Corbière, A., González-Dávila, M., Friedrich, T., Hauck, J., Heinze, C., Johannessen, T., Körtzinger, A., Metzl, N., Olafsson, J., Olsen, A., Oschlies, A., Padin, A., Pfeil, B., M.Santana-Casiano, J., Steinhoff, T., M.Telszewski, Rios, A. F., Wallace, D. W. R., and Wanninkhof, R.: Tracking the variable North Atlantic sink for atmospheric CO_2, Science, 326, 1391–1393, doi:10.1126/science.1177394, 2009.

Young, I. R., Zieger, S., and Babanin, A. V.: Global trends in wind speed and wave height, Science, 332, 451–455, doi:10.1126/science.1197219, 2011.

BGD
9, 10961–11012, 2012

Table 1. Estimates of anthropogenic CO_2 uptake by the oceans (Solomon et al., 2007).

Ocean-to-atmosphere anthropogenic CO_2 flux		
	Pg C yr^{-1}	uncertainty*
1980s	−1.8	0.8
1990s	−2.2	0.4
2000–2005	−2.3	0.4

* The uncertainty excludes interannual variability.

BGD
9, 10961–11012, 2012

Table 2. Summary of different components of the global-integrated net sea-air flux estimate including the sources and magnitude of the uncertainty.

	Year 2000 (from Takahashi et al., 2009)			Updated estimate[a]	
	Pg C yr^{-1}	%	Pg C yr^{-1}	Pg C yr^{-1}	Pg C yr^{-1}
Net flux	−1.38			−1.18	
ΔpCO_2		±13%	±0.18		±0.18
k		±30 %	±0.42		±0.2
Wind (U)		±20 %	±0.28		±0.15
$< \mathrm{d}(pCO_{2w})\ \mathrm{d}t^{-1}$[b]		±35 %	±0.5		±0.5
Total		±53 %	±0.7		
Under-sampling[c]	−0.2			−0.2	
Riverine carbon[d]	0.4		±0.2	0.45	±0.2
Coastal area				−0.18	
Anthro CO_2 flux	−2.0		±0.8[e]	−2.0	±0.6

For non El-Niño year 2000 (adapted from section 6, T-09).
[a] Details on the updated estimate are provided in the text.
[b] $\mathrm{d}(pCO_{2w})\ \mathrm{d}t^{-1}$ represents the error due to uncertainty in the mean rate of pCO_{2w} change of ($1.5 \pm 0.2\ \mu\mathrm{atm\ yr}^{-1}$) used for correcting observed values measured in different years to the reference year 2000.
[c] The bias due to spatial undersampling is determined by using the temperature bias of 0.08 °C between the measured SST used in the T-09 climatology and a comprehensive global SST climatology. For an iso-chemical temperature dependence of 4.2 % $°C^{-1}$ for pCO_{2w}, this translates into a pCO_{2w} bias of 1.3 μatm that in turn leads to a bias in global-integrated flux of −0.2 Pg C yr^{-1}. That is, the sink is greater when applying this correction.
[d] The CO_2 flux from riverine carbon input into the ocean is an efflux. To convert from the contemporary or net flux to the anthropogenic flux this value has to be subtracted. That is, the anthropogenic ocean CO_2 uptake is greater than the net flux derived from the T-09 climatology.
[e] Listed as ±1.0 in T-09.

BGD
9, 10961–11012, 2012

Table 3. Ocean General Circulation Models (OGCMs) with biogeochemistry[a].

Abbreviation	Name	Key Reference	Years used
BER	MICOM-HAMOCCv1	Assmann et al. (2010)	1990 to 2009
CSI	CSIRO-BOGCM	Matear and Lenton (2008)	1990 to 2009
BEC	CCSM-BEC	Doney et al. (2009a, b)	1990 to 2009
ETH_{k15}[b]	CCSM-ETH_{k15}	Graven et al. (2012)	1990 to 2007
ETH_{k19}[c]	CCSM-ETH_{k19}	–	1990 to 2007
LSC	NEMO-PISCES	Aumont and Bopp (2006)	1990 to 2009
UEA_{NCEP}[d]	NEMO-PlankTOM5$_{NCEP}$	Buitenhuis et al. (2010)	1990 to 2009
UEA_{ECMWF}[e]	NEMO-PlankTOM5$_{ECMWF}$	–	1990 to 2009
UEA_{CCMP}[f]	NEMO-PlankTOM5$_{CCMP}$	–	1990 to 2009

[a] For further detail on models refer to key reference and Canadell et al. (2012).
[b] ETH_{k15}: CCSM-ETH model with a prescribed global average gas transfer velocity of 15 cm h^{-1}.
[c] ETH_{k19}: CCSM-ETH model with a prescribed global average gas transfer velocity of 19 cm h^{-1}.
[d] UEA_{NCEP}: NEMO-PlankTOM5 model with NCEP core forcing.
[e] UEA_{ECMWF}: NEMO-PlankTOM5 model with NCEP core forcing but using ECWMF winds.
[f] UEA_{CCMP}: NEMO-PlankTOM5 model with NCEP core forcing but using CCMP winds.

BGD
9, 10961–11012, 2012

Table 4. Median anthropogenic CO_2 sea-air fluxes for the different approaches centered on year 2000.

Approach	Anthr. CO_2 flux	Uncertainty	IAV[e]	SAV[f]	Trend
	Pg C yr^{-1}	Pg C yr^{-1}	Pg C yr^{-1}		(Pg C yr^{-1}) $decade^{-1}$
Empirical	−2.0	±0.6[a]	0.20	0.61	−0.15
OGCM	−1.9	±0.3[b]	0.16	0.38	−0.14
Atm. Inversion	−2.1	±0.3[c]	0.40	0.41	−0.13
Ocean Inversion	−2.4	±0.3[d]			−0.5[j]
Interior (Green function)[g]	−2.2	±0.5	–	–	−0.35[j]
O_2 / N_2[h]	−2.2	±0.6			
O_2 / N_2[i]	−2.5	±0.7			

[a] Root mean square of uncertainty in individual parameters (see Table 2).
[b] Median absolute deviation of the six model outputs used to determine the median (for 6 model outputs: LSC, UEA_{NCEP}, CSI, BER, BEC and ETH_{k15}).
[c] Median absolute deviation of eleven model outputs used to determine the median.
[d] Median absolute deviation of the ten model outputs used to determine the median.
[e] Interannual variability (IAV) for the median values for the 6 models listed in[b].
[f] Subannual variability (SAV) for the median values (for 5 model outputs: LSC, UEA_{NCEP}, CSI, BEC and ETH_{k15}).
[g] Based on interior ocean changes using transient tracers and a Green function (Khatiwala et al., 2009, 2012).
[h] For 1993–2003 (Manning and Keeling, 2006).
[i] For 2000–2010 (Ishidoya et al., 2012).
[j] Calculated assuming steady ocean circulation and CO_2 uptake proportional to atmospheric CO_2 concentration.

BGD
9, 10961–11012, 2012

Table 5. Comparison of anthropogenic sea-air CO_2 flux, interannual and subannual variability of individual OGCM outputs used.

OGCMs	Provided flux[a] Pg C yr^{-1}	IAV[b] Pg C yr^{-1}	SAV[c] Pg C yr^{-1}	Trend (Pg C yr^{-1}) $decade^{-1}$
NEMO-PlankTOM5$_{NCEP}$	−2.08	0.20	0.32	−0.12
NEMO-PISCES	−1.93	0.22	0.32	−0.08
CSIRO-BOGCM	−1.93	0.21	0.51	−0.19
CCSM-BEC	−1.39	0.20	0.62	−0.17
CCSM-ETHk15[d]	−1.49	0.22	0.74	0.04
MICOM-HAMOCCv1	−2.58	0.45	3.32	−0.37
CCSM-ETHk19[d]	*−1.53*	*0.24*	*0.87*	*0.07*
NEMO-PlankTOM5$_{ECMWF}$	*−2.48*	*0.26*	*0.50*	*−0.24*
NEMO-PlankTOM5$_{CCMP}$	*−2.16*	*0.25*	*0.32*	*−0.05*

[a] This analysis is performed without the adjustment for a common ocean surface (Supplement A).
[b] IAV of median values: 0.16 (for 6 models: LSC, UEA$_{NCEP}$, CSI, BER, BEC and ETH$_{k15}$). The italicized models are excluded from the calculation of IAV and SAV in Table 4.
[c] SAV of median values: 0.38 (for 5 models: LSC, UEA$_{NCEP}$, CSI, BEC and ETH$_{k15}$). In addition to the italicized models, the MICOM-HAMOCCv1 is excluded in Table 4 as it shows extremely high SAV due to know model deficiencies.
[d] For the period of 1990–2007.

BGD
9, 10961–11012, 2012

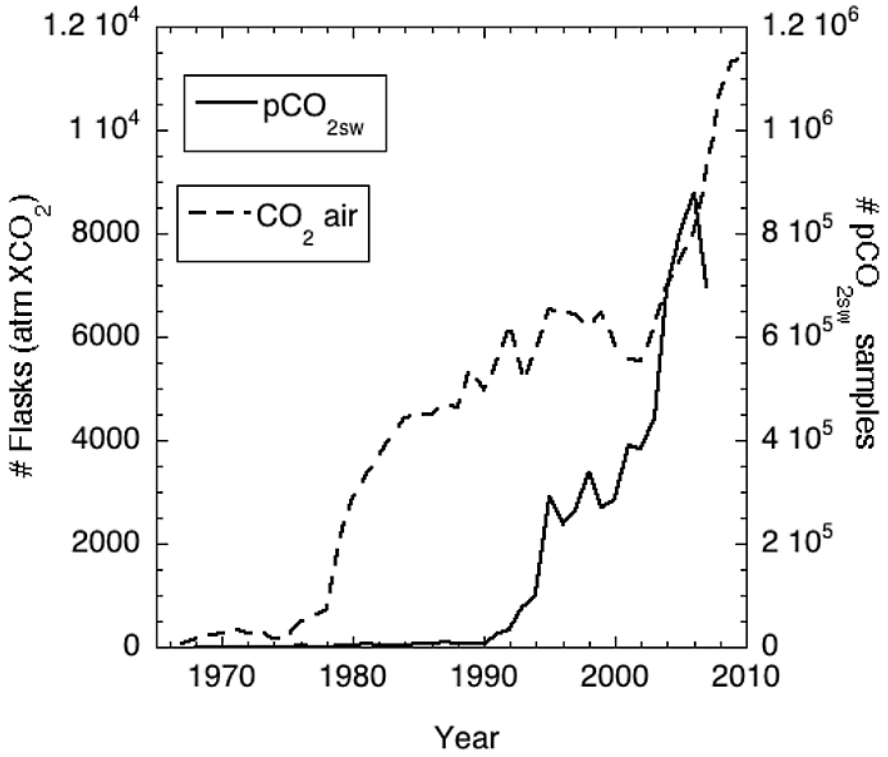

Fig. 1. Tabulation of the number of air CO_2 samples (dashed line, left axis) and surface water pCO_2 samples (solid line, right axis) taken per year. The tabulations for air samples are from NOAA/ESRL/GMD (courtesy T. Conway, NOAA/ESRL/GMD)) and the numbers of pCO_2 surface water samples are from the SOCAT database. Note the hundredfold difference in the scales of the left and right axes.

BGD
9, 10961–11012, 2012

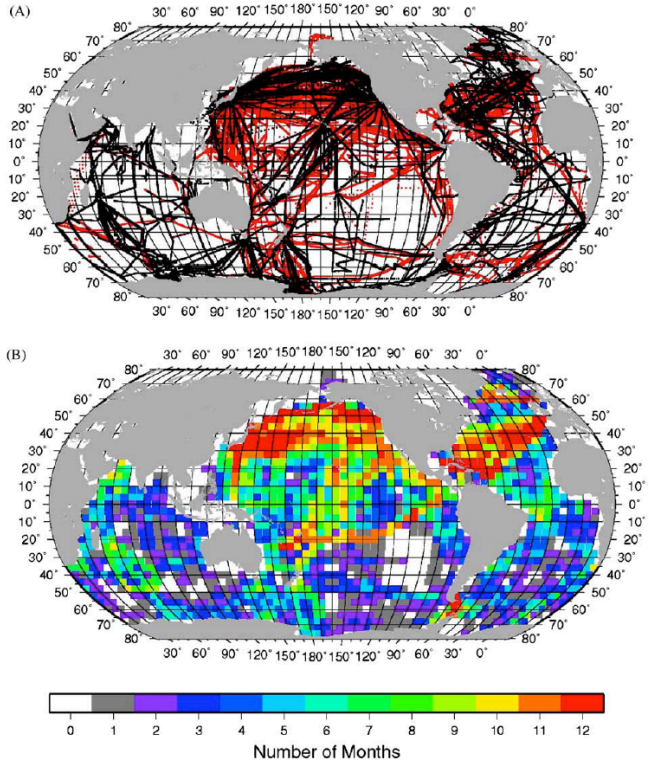

Fig. 2. (a) Cruise tracks with surface water pCO_2 measurements. The black lines indicate the tracks with measurements used in Takahashi et al. (2002) and the red lines are measurements added to the database in Takahashi et al. (2009). **(b)** Number of months in each 4° by 5° area where at least one surface water pCO_2 measurement has been made since the early 1970s. White areas are pixels that have no measurements. Reproduced from Fig. 1 in Takahashi et al. (2009).

BGD
9, 10961–11012, 2012

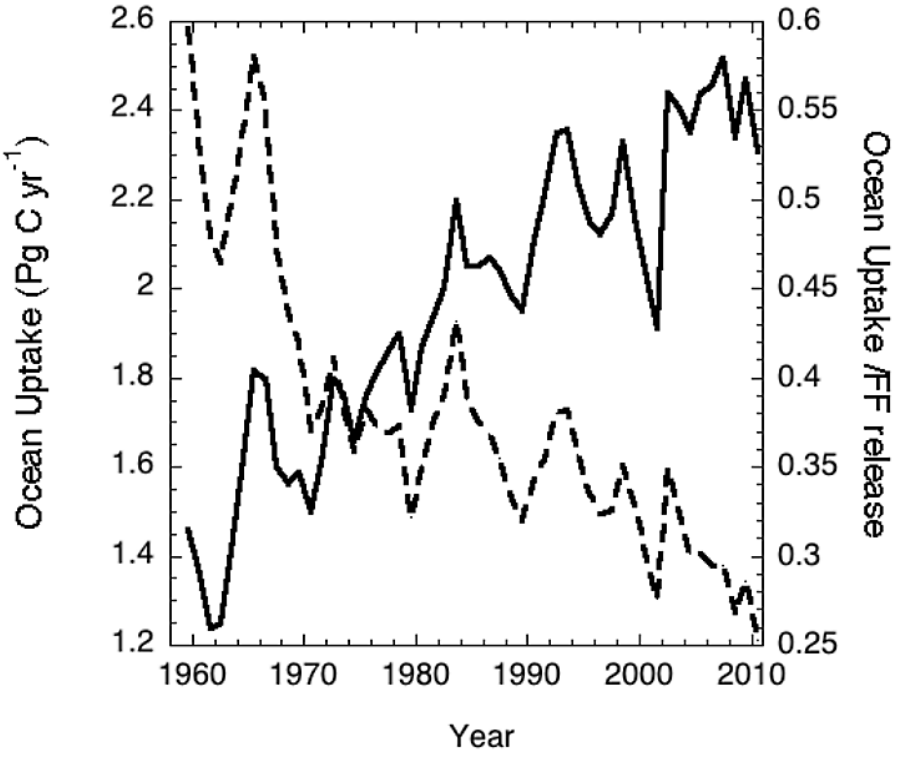

Fig. 3. Trend in global-integrated ocean CO_2 uptake based on an ocean model ensemble. The solid line (left axis) shows the increasing annual uptake while the dashed line (right axis) gives the decreasing fraction of fossil fuel CO_2 that is absorbed by the ocean. Data are from: http://www.tyndall.ac.uk/global-carbon-budget-2010#Jump%20to%20Data

BGD
9, 10961–11012, 2012

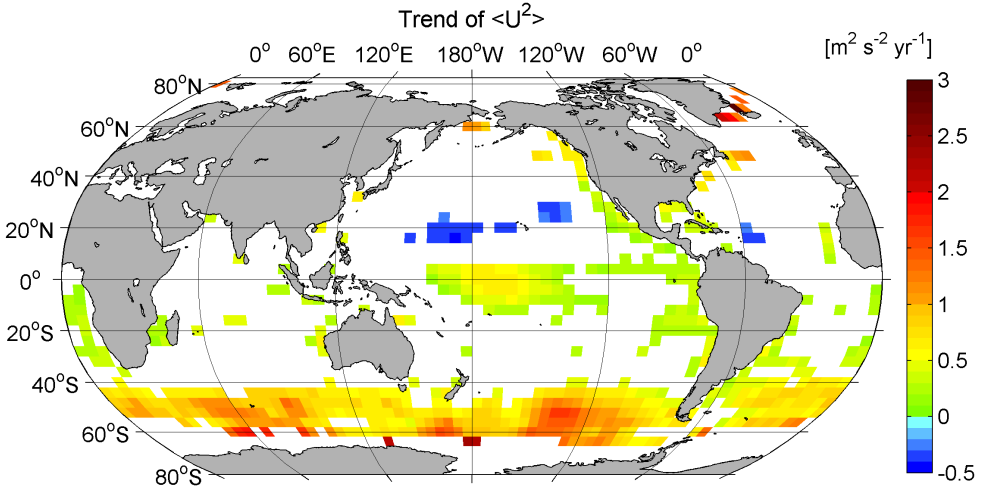

Fig. 4. Global spatial pattern of the temporal trend of the second moment of surface wind speed $\langle U^2 \rangle$ for the 20-yr CCMP wind product (1990–2009). Regions where trends are less than 90 % confidence level are masked.

BGD
9, 10961–11012, 2012

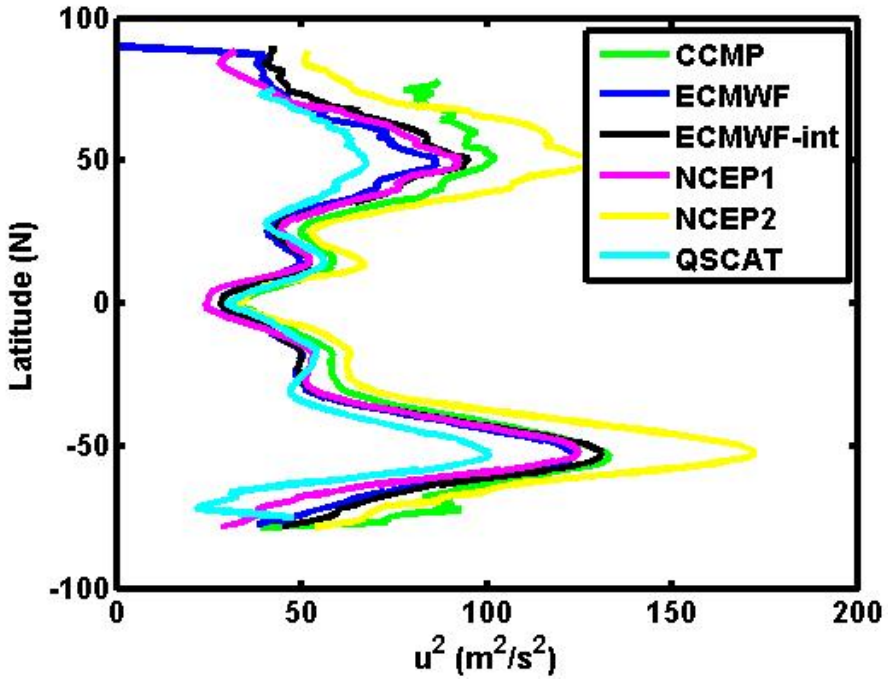

Fig. 5. Comparison of several global wind products showing the zonal mean distribution of the second moment of ocean surface winds for the year 2000. Differences of up to 30 $m^2 s^{-2}$ (wind speed difference $\approx 4\,m\,s^{-1}$) are observed, and the biases are not always consistent between high and low latitudes. CCMP = Cross Calibrated Multi-Platform winds (Atlas et al., 2011); ECWMF = European Center for Medium Weather Forecasting; NCEP = National Center for Environmental Prediction; QSCAT = QuikSCAT polar orbiting satellite with an 1800 km wide measurement swath on the earth's surface equipped with the microwave scatterometer SeaWinds.

BGD
9, 10961–11012, 2012

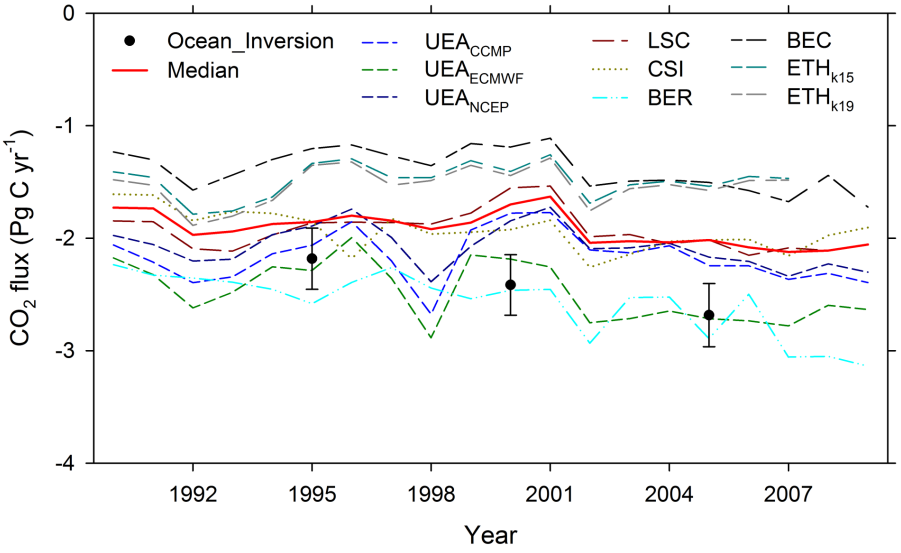

Fig. 6. Summary of annual global-integrated sea-air CO_2 fluxes from the ocean general circulation models, OGCMs (dashed lines), and ocean inversion estimate (circles with uncertainty bars). Similar line types for the OGCMs indicate that the models have the same heritage. The median (solid red line) is the median of UEA_{NCEP}, LSC, CSI, BER, BEC and ETH_{k15}.

BGD
9, 10961–11012, 2012

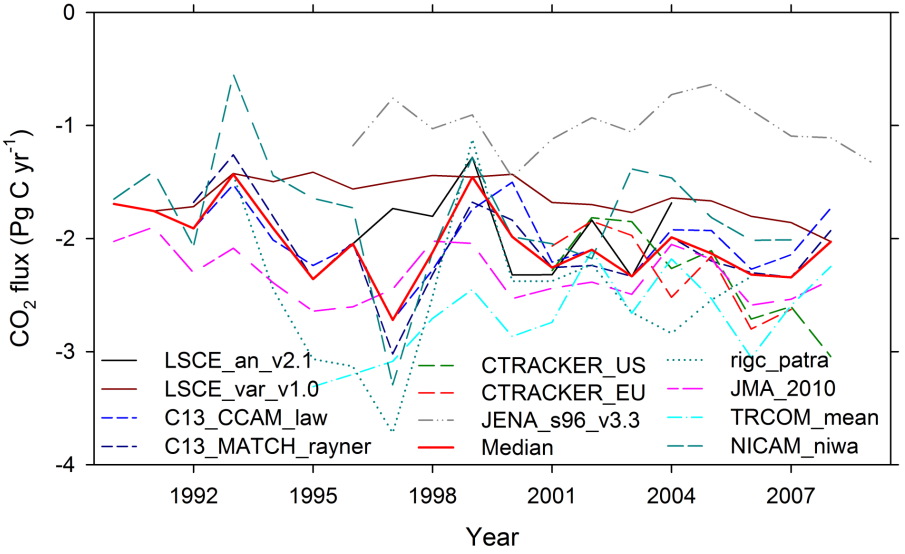

Fig. 7. Summary of annual global-integrated sea-air CO_2 fluxes from atmospheric inverse models. The red line is the median of all models shown.

BGD
9, 10961–11012, 2012

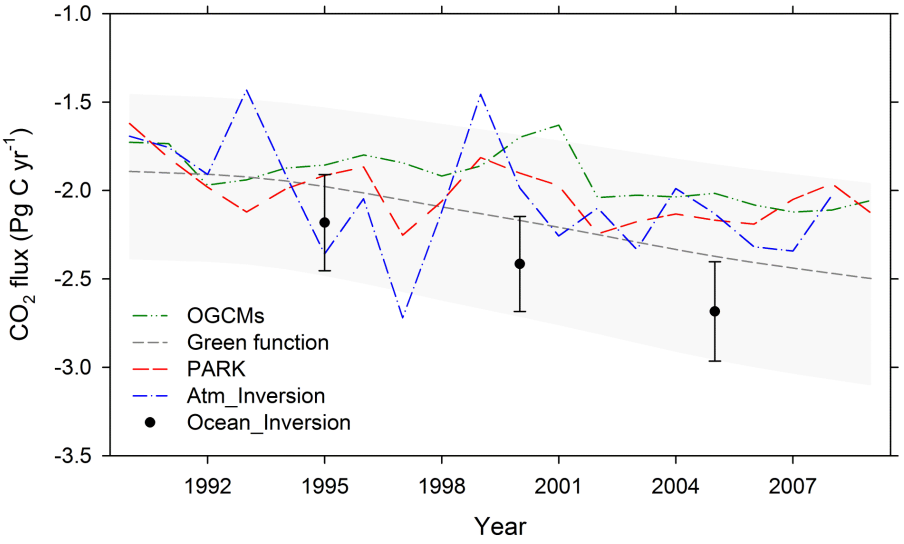

Fig. 8. Summary of the different modeling approaches. In case of the OGCMs and atmospheric inverses, the annual median value is plotted.

BGD
9, 10961–11012, 2012

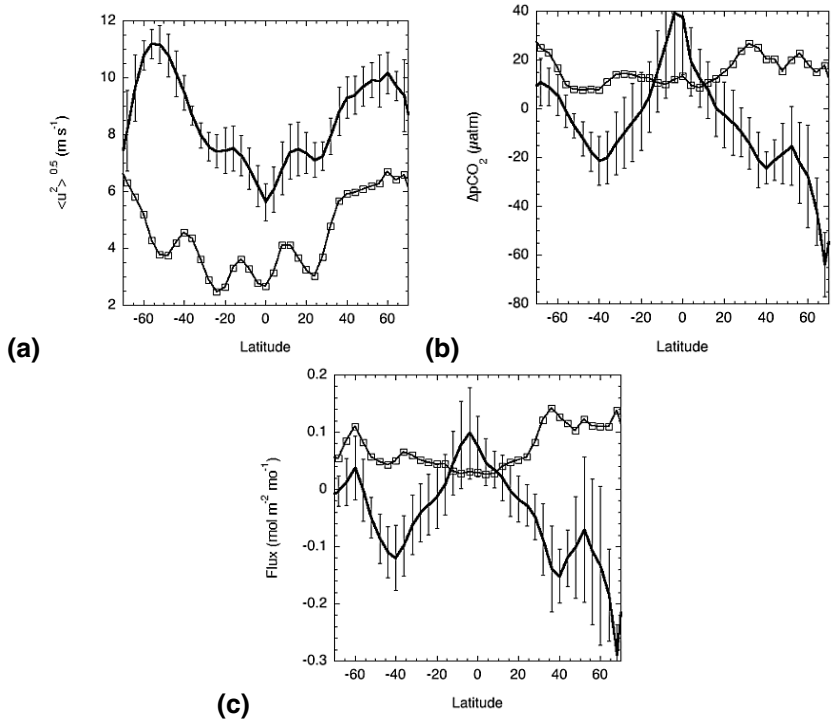

Fig. 9. Latitudinal distribution of zonal means (thick solid line) and standard deviations (spatial and temporal variability) (thin solid line with squares) for the: **(a)** square root of the second moment $\langle U^2 \rangle^{0.5}$ of the 20-yr monthly mean CCMP wind product; **(b)** ΔpCO_2 from the monthly Takahashi et al. (2009) climatology; and **(c)** the specific air-sea CO_2 flux [mol m^2 mo^{-1}] computed by applying the 20-yr CCMP wind product to the Takahashi pCO_{2w} climatology using Eq. (2). The error bars on the zonal means indicate the spatial variability (standard deviation) of means for the 5° longitude bins in the particular latitude band.

BGD
9, 10961–11012, 2012

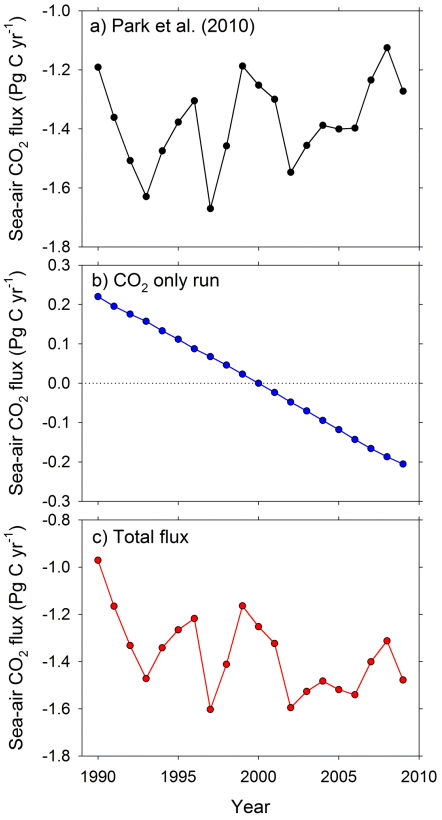

Fig. 10. (a) Global-integrated sea-air CO_2 fluxes versus time determined with the empirical approach of Park et al. (2010a); **(b)** the global-integrated anomaly of sea-air flux caused by increasing atmospheric CO_2 based on the BEC ocean model output and referenced to year 2000; **(c)** the net global-integrated sea-air flux based on the empirical approach and the BEC CO_2-only run.

BGD
9, 10961–11012, 2012

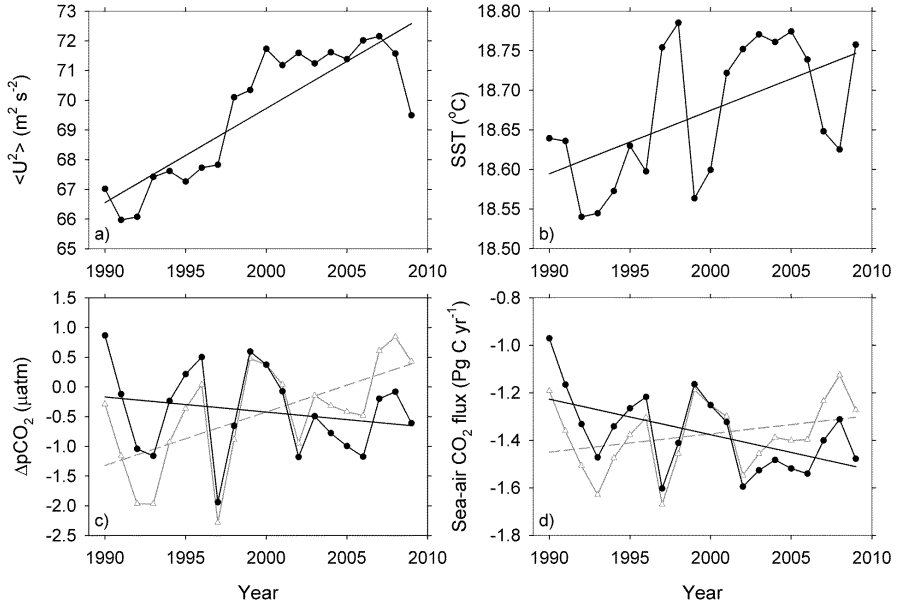

Fig. 11. Global ocean trends in: **(a)** second moment of wind speed; **(b)** SST; **(c)** ΔpCO_2, assuming no atmospheric CO_2 increase (gray line) and including atmospheric CO_2 forcing (black line); and **(d)** global-integrated sea-air CO_2 flux over the past two decades (1990-2009) without atmospheric CO_2 forcing (gray line) and with atmospheric CO_2 forcing (black line). The change in ΔpCO_2 is determined according to the procedures of Park et al. (2010a). The slopes for the linear regressions (solid line) for area-weighted $\langle U^2 \rangle$, SST, ΔpCO_2 and flux are 0.32 ± 0.04 $(\mathrm{m\,s^{-1}})^2\,\mathrm{yr^{-1}}$; 0.08 ± 0.03 $(^\circ\mathrm{C\,yr^{-1}})$ $\mathrm{decade^{-1}}$; -0.3 ± 0.3 $(\mu\mathrm{atm\,yr^{-1}})$ $\mathrm{decade^{-1}}$ including atm CO_2 forcing; and -0.15 ± 0.06 $(\mathrm{Pg\,C\,yr^{-1}})$ $\mathrm{decade^{-1}}$ including atm CO_2 forcing, respectively.

BGD
9, 10961–11012, 2012